AD-A061 147 ARMY ELECTRONICS RESEARCH AND DEVELOPMENT COMMAND FO--ETC F/G 9/1
LOW-COST, CROSSED-FIELD AMPLIFIER MEANDERLINE CIRCUIT CONCEPTS.(U)
AUG 78 C D BATES, J H HARTLEY

UNCLASSIFIED DELET-TR-78-18 NI

1 OF 1
AD
A061147

END
DATE FILMED
1-79
DDC

(13)

LEVEL II

RESEARCH AND DEVELOPMENT TECHNICAL REPORT

DELET-TR-78-18

LOW-COST, CROSSED-FIELD AMPLIFIER MEANDERLINE CIRCUIT CONCEPTS

Calvin D. Bates
Joseph H. Hartley

ELECTRONICS TECHNOLOGY & DEVICES LABORATORY

August 1978

ERADCOM

US ARMY ELECTRONICS RESEARCH & DEVELOPMENT COMMAND
FORT MONMOUTH, NEW JERSEY 07703

NOTICES

Disclaimers

The citation of trade names and names of manufacturers in this report is not to be construed as official Government indorsement or approval of commercial products or services referenced herein.

Disposition

Destroy this report when it is no longer needed. Do not return it to the originator.

UNCLASSIFIED

SECURITY CLASSIFICATION OF THIS PAGE *(When Data Entered)*

REPORT DOCUMENTATION PAGE

READ INSTRUCTIONS BEFORE COMPLETING FORM

1. REPORT NUMBER: DELET-TR- 78-18	2. GOVT ACCESSION NO.
3. RECIPIENT'S CATALOG NUMBER	
4. TITLE *(and Subtitle)*: Low-Cost, Crossed-Field Amplifier Meanderline Circuit Concepts.	5. TYPE OF REPORT & PERIOD COVERED: Research and development Technical Report.
6. PERFORMING ORG. REPORT NUMBER	
7. AUTHOR(s): Calvin D. Bates and Joseph H. Hartley	8. CONTRACT OR GRANT NUMBER(s)
9. PERFORMING ORGANIZATION NAME AND ADDRESS: USA Electronics Technology & Devices Lab. (ERADCOM) Fort Monmouth, N.J. 07703	10. PROGRAM ELEMENT, PROJECT, TASK AREA & WORK UNIT NUMBERS: 1L1 62705 AH94 B1 17 16
11. CONTROLLING OFFICE NAME AND ADDRESS: Beam, Plasma and Display Division US Army Electronics Technology and Devices Lab (ERADCOM) ATTN: DELET-BM	12. REPORT DATE: August 1978
	13. NUMBER OF PAGES: 52
14. MONITORING AGENCY NAME & ADDRESS *(if different from Controlling Office)*: 59 p.	15. SECURITY CLASS. *(of this report)*: Unclassified
	15a. DECLASSIFICATION/DOWNGRADING SCHEDULE

16. DISTRIBUTION STATEMENT *(of this Report)*

Approved for public release; distribution unlimited.

17. DISTRIBUTION STATEMENT *(of the abstract entered in Block 20, if different from Report)*

18. SUPPLEMENTARY NOTES

19. KEY WORDS *(Continue on reverse side if necessary and identify by block number)*

Meanderline	S-Band
Low-cost	Arc-plasma-spray (APS)
Crossed-field amplifier (CFA)	Direct-bonded-copper (DBC)
Microwave amplifier	Interaction impedance
L-Band	Laser-cut

20. ABSTRACT *(Continue on reverse side if necessary and identify by block number)*

Experimental results of new, potentially low-cost, crossed-field amplifier (CFA) anode circuits are presented and compared with state-of-the-art structures. The shaped-substrate meanderline (SSML) has emerged as the optimum choice for achieving the desired low-cost objectives without compromising the excellent electrical characteristics of available injected beam CFA's (IBCFA). L-Band and S-Band meanderline circuits were designed and constructed on primarily low-dielectric constant substrates. Design aspects were investigated

DD FORM 1 JAN 73 1473 EDITION OF 1 NOV 65 IS OBSOLETE

UNCLASSIFIED

SECURITY CLASSIFICATION OF THIS PAGE *(When Data Entered)*

410 698 LB

#20 (ABSTRACT (Contd.)

to optimize bandwidth and interaction impedance while maintaining simplified, low-cost structures. Circuit fabrication techniques using arc-plasma-sprayed (APS) spinel were evaluated and found deficient in the areas of low circuit attenuation and surface regularity. Laser machining techniques, which will be covered in another report, have recently emerged as the most promising approach for resolving SSML fabrication problems, and achieving low-cost circuit structures. A simulated, SSML, S-Band, anode design on beryllia dielectric was formulated and subsequently utilized by Northrop Corporation in a contractual effort to verify the circuit design in an operational CFA. Results of that hot-test are presented.

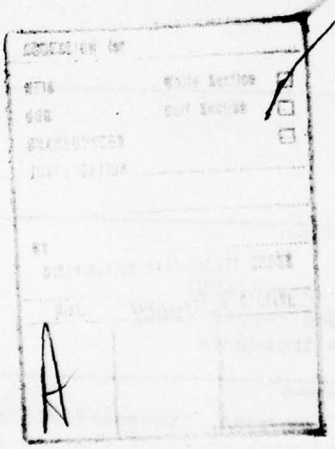

CONTENTS

FIGURES

CONTENTS (Continued)

CONTENTS (Continued)

TABLES

LOW-COST, CROSSED-FIELD AMPLIFIER MEANDERLINE CIRCUIT CONCEPTS

INTRODUCTION

This report describes the initial results of an internal effort at ERADCOM to investigate interaction structures for medium-power, microwave, crossed-field amplifiers (CFA's). Since the emergence of the CFA in the late 1950's there has been a steady improvement of this tube type, and a corresponding increase in its military applications. The overall program objective is to develop anode circuit concepts that lead to medium-power CFA's with performance equivalent to the best commercially avaliable devices, and exhibit the potential for achieving low-cost production. The internal program has been limited to the development of circuit concepts and associated cold test experimentation to verify performance. One of the circuit concepts was subsequently selected for hot test implementation at an industrial facility.

The primary cost barrier in available moderate-power CFA's is the expensive fabrication procedures and inherent design complexity associated with the anode interaction structures. Extensive studies[1] funded by ERADCOM have indicated that even in high volume production the piece-part anode structure would have a unit cost of approximately $1000, which drives the finished tube cost to the $2000-3000 level, and thus eliminates the device as a candidate for most Army Electronic Warfare (EW) and phased array radar applications. This program has an anode cost goal of $200 or less.

The requirement for low-cost, high-performance microwave amplifiers resulted in an ERADCOM effort to investigate and develop alternate anode circuit design concepts with potential for low manufacturing cost, without sacrificing the excellent bandwidth, power, and efficiency performance found in the conventional high-cost CFA structures. During the course of this effort many circuit designs and fabrication approaches were investigated to ascertain their potential for replacing the more costly anode circuits. The need to reduce costly piece-part fabrication concepts was used as the guide for generating new anode designs. The fabrication problems associated with some of the circuits have been recently resolved by utilizing precision laser machining of the circuit substrate. The laser-cut technique permits the design and fabrication of anode circuits consisting of only a few parts, and has the potential for costing less than $200 in production. This most promising fabrication procedure will be the subject of a subsequent report describing design details, and operational characteristics.

MEDIUM-POWER CROSSED-FIELD AMPLIFIERS (CFA's)

As is common with other microwave tube types, there are high and medium-power CFA's. Other microwave tube types have low-power versions, and while a low power CFA is possible, it would not be competitive with other types of microwave tubes. Typical medium-power CFA's provide peak power outputs of 20 kilowatt (kW) at 10 percent duty, or 2kW, continuous wave (CW) output

---

1. H. L. McDowell, "Ceramic Mounted Circuit for Crossed-Field Amplifiers," ECOM-0273-F, Contract No. DAAB07-72-C-0273, March 1974.

in S-Band, 2-4 Gigahertz (GHz). At other frequencies, medium-power would be defined by applying the power frequency scaling relationship (pf^2) to the above cited S-Band values. In some applications it is desirable to have both pulsed and CW capability in the same tube, and such a dual-mode, medium-power CFA has been used in important military ECM applications.

Figure 1 shows a schematic depiction of a typical linear-format, injected-beam CFA configuration discussed in this report. An essential requirement for this device is that the electron beam velocity be synchronous with the phase velocity of the radio-frequency (RF) wave on the anode circuit. Under this condition the RF wave gains energy at the expense of the electron beam energy. The anode circuit length is chosen to optimize gain and the circuit dispersion determines the instantaneous operating bandwidth. The anode circuit is subject to considerable beam interception (inherent in the crossed-field interaction process) which necessitates adequate anode circuit thermal dissipation capability. After leaving the anode/sole interaction region the residual beam energy is dissipated at the collector.

The medium-power CFA is further differentiated into backward-wave and forward-wave devices, each exhibiting specific advantages and disadvantages with regard to instantaneous bandwidth, voltage tunability, gain, power handling capability and efficiency. The inherent nature of the interaction process in the backward-wave CFA limits the instantaneous bandwidth to a few megahertz (MHz). The low-cost CFA program objectives dictate broad instantaneous bandwidth, hence backward-wave structures were excluded from this study.

Medium-power, forward-wave CFA's are commercially available in both S- and C-bands with CW output power levels of 2kW and 1kW respectively. However, these devices use high-cost, complex anode structures to obtain broad instantaneous bandwidth with moderate gain, 20 decibel (dB), and excellent efficiency (50 percent). These devices have restricted use due to their high-cost, but the excellent performance outweighs the cost disadvantage in some military applications. The complex circuit fabrication and assembly procedures required to construct the presently used shielded meanderline (Figure 2) cause this circuit to be expensive. As shown in the figure, piece-part construction is necessary and hundreds of parts must be precisely aligned during the brazing operations. The mismatch in thermal expansion coefficients between copper and beryllia (BeO) adds further complications.

In high and medium-power CFA's a variety of anode circuits have proven successful and the meanderline has emerged as the optimum medium-power anode structure for obtaining the desired broad bandwidth. The meanderline represents a close approximation to the helix structure widely used in traveling wave tubes (TWT's). The low dispersion and adequate coupling impedance of the helix are generally exhibited in the meanderline structure. The most important advantage of the meanderline over the helix is increased thermal capability. The intimate thermal contact between the circuit and the ground plane provides the heat dissipation required for moderate power operation. This design aspect is of extreme importance since the crossed-field anode structure must collect significant amounts of beam current under operating conditions. For conservative tube design the anode circuit should be able of dissipating approximately 50 percent of the direct current (dc) power.

CIRCUIT MEASUREMENT TECHNIQUES

The electrical measurements of the circuits designed and constructed during this program are essentially the same for all the experimental circuits, and before discussing in detail the electrical performance of the circuit structures, it would be beneficial to review the parameters measured, and the procedures used to insure the validity of the measurements. Table 1 lists the most important electrical parameters that are determined during tests on experimental models. All of the parameters tabulated are frequency dependent, therefore, accurate frequency measurements were designated the highest priority. An electronic frequency counter with a transfer oscillator was utilized for the frequency measurements. This instrument has a digital readout and seven place accuracy is routinely attained. Identification of resonances, where necessary, was accomplished with a network analyzer and auxilliary polar and phase/gain indicators. The first measurements are usually made to determine the circuit delay factor τ where

$$\tau = c/v_p \qquad (I)$$

c is the speed of light, 2.99792×10^8 meters/second
and v_p is the phase velocity of the circuit.

This parameter normally has a value between 10 and 20 for practical CFA's. The frequency dependence of τ is a measure of dispersion and indicates the operating instantaneous bandwidth of the CFA. Two similar measurement procedures are in use for determining τ, differing only in the method of RF coupling to the circuit structures to obtain measurements of the resonant frequencies. In this program the meanderline circuit was directly coupled to the test signal source. A matched RF input connector is attached to the circuit, leaving the output connector open-circuited to resonate the structure. At the fundamental quarter-wave resonance of the open-ended circuit, the input appears short circuited. This same condition prevails for all odd multiples of $\pi/2$ radians phase shift, and a table of resonant frequencies is prepared along with the total circuit phase shift at each resonant point. The value of τ is then calculated using the expression

$$\tau = \frac{c}{v_p} = \frac{\theta_\ell}{\theta_o} \qquad (2)$$

where, θ_ℓ is the cumulative phase shift from meanderline input to output and θ_o is the corresponding free-space phase shift in the same distance. The phase velocity v_p can be readily calculated from the experimentally determined value of τ.

An approximate circuit group velocity v_g can be calculated from the previously tabulated τ data by using the expression,

$$v_g = \frac{2\pi\ (f_1 - f_2\ )\ p}{\theta_1 - \theta_2} \tag{3}$$

where, f_1, and f_2 are the successive odd quarter-wave resonances, θ_1 and θ_2 are the corresponding vane-to-vane phase shift values measured at f_1 and f_2 respectively, and p is the pitch. (In a non-dispersive media, the phase velocity and group velocity are equal).

This calculated value of group velocity v_g is a close approximation to the exact value at the frequency midway between f_1 and f_2. The exact value is the derivative, expressed as,

$$\left.\frac{df}{d\theta}\right]_{\theta} = \frac{\theta_1 + \theta_2}{2} \tag{4}$$

where $\frac{\theta_1 + \theta_2}{2}$ is the midpoint phase shift value.

Having determined v_p and v_g, the interaction impedance K_i, sometimes referred to as the beam coupling impedance, can be measured using a perturbation technique as described in the literature by P.N. Hess[2]. In this method a low-loss, thin dielectric sheet is placed in contact with the surface of the microwave structure under investigation. The frequency of the odd quarter-wave resonances previously measured is shifted slightly, and this change in frequency is recorded. In general, the perturbation sheet is kept as thin as possible to produce small changes in frequency while at the same time achieving intimate contact with the circuit. The interaction impedance is then calculated using the following expression by Hess with terms rearranged for convenience,

$$K_i = 2\,\frac{\ell g}{ht}\,\frac{m^2}{\theta^2\ v_g\ \varepsilon_o\ (\varepsilon_r - 1)}\,\frac{\Delta f}{f} \tag{5}$$

---

2. P. N. Hess, H. Kohlmoos, Jr., "Study of Interaction Structures," Technical Report ASD-TDR-62-813, Contract AF 33(616)-8078, Nov 1963.

where the geometrical constants are defined as follows, (see also Figure 3)

ℓ - circuit pitch
g - gap or slot width
h - width of perturbing dielectric sheet (comparable to electron beam width)
t - thickness of the perturbing dielectric sheet (0.05 millimeter (mm), mylar used in this study)

and, the electrical symbols are defined as tabulated below,

ε_o - free space permittivity ($\frac{1}{36\pi} \times 10^{-9}$ farads/meter)

ε_r - relative permittivity of the perturbing dielectric, ($\varepsilon_r = 2.8$ for Mylar)

v_g - group velocity at frequency f in meters/second

θ - phase shift per pitch in radians at frequency f.

Δf - frequency shift due to dielectric perturbation in MHz

f - odd quarter-wave resonant frequency in MHz before perturbation

$m - \frac{\sin \theta \frac{g}{\ell}}{\theta \frac{g}{\ell}}$.

Gap-factor (m^2/θ^2) tables were also prepared for each of the circuits tested and were utilized to simplify the calculations.

A block diagram of the test equipment arrangement for v_p, v_g, and K_i measurements is depicted in Figure 4.

The propagation constant β is directly derived from v_p by the expression,

$$\beta = \frac{2\pi f}{v_p} \qquad (6)$$

where, f is the frequency at which the phase velocity v_p is measured. Characteristic impedance Z_o is measured by means of a time domain reflectometer. This instrument also serves to evaluate the RF match of the input and output connectors, and provides a qualitative measure of geometrical imperfections in the meanderline.

Attenuation or circuit RF loss, and voltage-standing-wave-ratio (VSWR), are measured with a frequency response test set in which reflected and transmitted power are compared to a reference level derived from the incident test signal. A precision dual directional coupler and broadband video detectors are used to provide the input to the frequency response test set.

The theoretical value of attenuation is obtained by using the microstrip theory provided by M. Caulton[3]. The following expression for the attenuation per unit length was used for the experimental circuits.

$$\alpha = (8.686)\ \frac{R_{s1} + R_{s2}}{2Z_o\ W} \qquad (7)$$

where α is the attenuation in dB/meter
R_{s1} is the surface resistivity* of the metallic meanderline (ohms)
R_{s2} is the surface resistivity of the metallic ground plane (ohms)
Z_o is the measured characteristic impedance of the circuit (ohms)
w is the width of the conducting meanderline strip (meters)

* (or high-frequency skin effect resistance)
R_s for copper = $2.61 \times 10^{-7} \sqrt{f}$ where f = frequency of operation.

If the metallic meanderline and the metallic ground plane are constructed of the same material then Equation (7) becomes:

$$\alpha = (8.686)\ \frac{R_s}{Z_o W} \qquad (8)$$

EXPERIMENTAL RESULTS

1. Continuous Substrate Meanderlines (CSML)

The prototype meanderline with dimensional definitions is shown in Figure 3. Inclusion of a dielectric substrate and a ground plane as in Figure 5 leads to the CSML configuration. A photograph of this type of circuit is also shown in Figure 6. The thickness and dielectric constant of the substrate material determines to a large extent the important electrical and RF characteristics of the resultant CSML. It can be seen that the CSML is essentially a microstrip transmission line following a serpentine path. The microstrip theory as developed by M. Caulton was used throughout the program for calculation of major circuit parameters.

At first glance the CSML would appear to be a strong candidate for a low-cost anode structure. A ceramic substrate material clad with copper on both sides could be subjected on one surface to a photolithographic process which would generate the meanderline, and the opposite copper surface would serve as a ground plane. This anode circuit structure would

---

3. M. Caulton, et al., "Measurements on the Properties of Microstrip Transmission Lines for Microwave Integrated Circuits," RCA Review, Vol. 27, No. 3, Sep 1966.

certainly be low-cost, and to a great extent, meet the electrical and thermal requirements of a CFA anode structure. The one deficiency which prevents the use of the CSML is the sputtering problem encountered in the crossed-field tube. The small anode-to-sole spacing (Figure 1), and intense electrical and magnetic fields present, cause sole-material to be readily sputtered onto the anode circuit. In short order, a conducting film sputtered from the sole covers the interaction gaps (anode slots) and renders the tube inoperative. In recent years the sputtering problem has been relieved to some extent by use of a refractory metal carbide or boride coating on the sole. This permits the CSML to be considered for shorter life tubes such as expendable jammers whose operational times are usually far less than the time required to experience the effects of sputtering. The CSML was investigated during this program because it is easy to fabricate, and serves as a standard by which to judge the microwave performance of alternate design concepts.

a. L-Band CSML on Polyguide Dielectric

Two experimental CSML's were constructed on this program, and the first of these is depicted in Figures 5 and 6. The circuit is designed to operate in L-Band (1-2 GHz) with an irradiated polyethylene (polyguide) substrate material which has the low relative dielectric constant (ε_r) of 2.3. It is important to note that this dielectric material is not suitable for actual hot test vehicles due to it's plastic nature. However, this program deals with the analysis of both hot and cold test circuit configurations to achieve new design concepts which can be fabricated later using proper dielectric materials such as alumina or beryllia. In most cases the use of low-loss, plastic dielectric substrates for cold test analysis is more cost-effective for studying various anode circuit designs and concepts. The circuit fabrication was relatively straightforward, a piece of standard, copper-clad polyguide microwave substrate serving as the starting point. The original dielectric thickness of 1.5 mm was reduced by machining to the desired 0.64 mm dimension. Photolithographic techniques were used to form a meanderline by etching the 0.04 mm thick copper layer remaining on one side of the polyguide. The intermediate assembly which consisted of a conducting meanderline on dielectric substrate, was bonded to a copper ground plane, and 50 ohm RF input and output connectors were installed to complete the structure. The geometrical parameters for this circuit are listed in Table 2.

The frequency dependent parameters for the CSML on polyguide were determined by performing the previously discussed measurements, and processing the experimental data using the analytical expressions covered in the measurements section. The information is presented in graphical form in figures 7, 8, and 9. The characteristic impedance Z_o was found to be 55 ohms, which is close to the 50 ohm design value. The fabrication procedure did not yield the exact 1:1 metal-to-space ratio, and the dielectric thickness was 0.1 mm oversized. The affects of these two fabrication errors tend to cancel, since the wider conducting strip lowers Z_o and the thicker dielectric substrate raises Z_o.

The delay factor $\tau=(c/v_p)$ is in agreement with the microstrip calculations at low frequency if the wider conducting strip is taken into account. The theory used does not permit dispersion to be calculated, so this circuit constant is determined experimentally. The dispersion, shown in Figure 7, is evidenced by an increase in the phase delay (or slowing) factor with frequency, and is a result of greater concentration of the electric field in the dielectric and a corresponding increase in the effective dielectric constant of the media surrounding the meanderline. A non-dispersive circuit or transmission line would appear as a horizontal line with a constant delay factor over the entire range of phase shifts. A close approximation of the operating instantaneous bandwidth of the circuit can be determined from Figure 7 using the following steps. First, the mid-band frequency, or phase-shift, which corresponds to that frequency is selected, and a vertical line is drawn from that frequency intersecting the c/v_p curve. For the purpose of this example, F = 1.5 GHz (or phase shift $\theta = 80°$) was selected as a convenient starting point. Secondly, a horizontal line (signifying a constant electron beam velocity, required during instantaneous bandwidth operation) is drawn through the point of intersection of the vertical frequency line and the c/v_p curve. In this example the intersection occurs at a c/v_p value of 14.1. In practice the instantaneous bandwidth of a linear-beam CFA device can be obtained over a range of $\pm$ 3 percent from beam/circuit wave synchronism. The operating point or beam velocity of the device is set at an optimum value for achieving bandwidth and power output by selecting the appropriate values of beam voltage and magnetic field. In this instance the value of 14.1 was selected. Calculating the delay factor $(c/v_p) \pm 3$ percent results in two new values for c/v_p. In this case they are $c/v_p = 14.5$, and $c/v_p = 13.7$. These new values of c/v_p are used to determine the upper and lower operating frequency, and the difference between these frequencies is considered the instantaneous bandwidth. To complete this example, Figure 7 indicates that an instantaneous bandwidth of 1200 MHz, or greater than one octave, can be achieved with this circuit structure under hot test conditions. There are many other operational factors which influence the instantaneous bandwidth capability of a CFA, but in general practice, the aforementioned approximation is valid.

The circuit attenuation is shown in Figure 8. The total RF attenuation of the circuit is the sum of the ohmic losses in the metallic conductors and the dielectric losses in the substrate. The total RF loss measured was almost entirely due to the conducting media losses, and agrees with the calculated value of loss contributed by the circuit conductor. Dielectric loss was also calculated and found to be less than 1 percent of the total RF attenutation value, and in most cases can be ignored. The circuit loss at a desired frequency can also be specified as a function of the conductor strip length to provide a more meaningful comparison to other circuits. At a frequency of 1.5 GHz this circuit exhibited an attenuation value of 1.03 dB per meter.

In Figure 9 the interaction impedance K_I is plotted as a function of phase shift per section θ. The range of values is comparable to those found in commercial tubes presently in use. The circuit VSWR was found to be 1.22:1 and represents a very close approximation to the theoretical

value of 1.2:1 for the mismatch between a 55 ohm transmission line and a 50 ohm measurement system.

b. S-Band CSML, Direct-Bonded-Copper (DBC) on Alumina Dielectric

The other CSML constructed on this program was an S-Band design with an alumina (AL_2O_3) dielectric substrate having a relative dielectric constant (ε_r) of 9.6, and is shown in Figures 10 and 11. A dielectric plate (coupon) with copper bonded to both sides is processed by photolithographic means to yield the meanderline-ground plane assembly. The copper was bonded directly to the alumina substrate surfaces by a new technique[4] which uses high temperature and a controlled oxygen containing atmosphere to bond copper to the substrate without the need for premetallization with other materials. This new process, designated direct-bonded-copper is also being investigated for ultimate use in the manufacturing of microwave devices. In its present stage, the process exhibits some deficiencies related to bonding voids and surface abnormalities, which must be improved so that precision circuits with high thermal capability can be fabricated. It should also be mentioned here, that the bonded interface layer may contain significant amounts of oxygen which would curtail the use of hydrogen atmosphere brazing processes during hot test device fabrication. The entire bonding process, and the bonded interface area must be studied further in order to exploit this new bonding technology and realize its full low-cost potential for microwave devices. This circuit served to supplement this program by providing additional CSML data in which L-Band geometrical circuit constants were scaled to S-Band, and higher dielectric substrate materials were used. The circuit as shown in Figure 11 has been photoetched to create the meanderline configuration. The edges of each circuit section indicate tapering, which is due to the photoetching of the thick (0.25 mm) metallic layer. The connectors shown are typical 50 ohm SMA bulkhead types, and were used as an expedient method to obtain electrical performance. Two 0.25 mm diameter copper wires were also used to provide RF connections to each end of the meanderline circuit. The geometrical parameters for this circuit are listed in Table 3.

The electrical performance information is graphically presented in Figures 12, 13, and 14. The dispersion curve for this circuit, shown in Figure 12, indicates a narrowing of the instantaneous bandwidth capability, and a higher delay factor in comparison to the prior circuit. Both of these values are affected by the higher dielectric constant of the substrate material. Also, the increased capacitance from vane-to-vane (caused by the thick metallic conductor), and the high dielectric intervane loading tend to further reduce the instantaneous bandwidth. The increased delay factor is almost entirely due to the high dielectric constant of alumina. The instantaneous bandwidth is calculated using the example in the preceding section. Selecting the center frequency of 2.5 GHz, and calculating c/v_p for the $\pm$ 3 percent points produces an instantaneous bandwidth of only 350 MHz. This value can also be expressed as a percentage of the center frequency, which in this case would be 14 percent instantaneous bandwidth.

4. Y. S. Sun, J. C. Driscoll, " A New Hybrid Power Technique Utilizing a Direct Copper to Ceramic Bond," IEEE Trans. Electron Devices, Vol. ED-23, No. 8, pp. 961-967, August 1976.

The preceding L-Band circuit exhibited more than 80 percent instantaneous bandwidth. The alumina circuit may be suitable for radar type bandwidth applications, but would not fulfill the requirement for broadband CFA circuits.

This circuit exhibited RF loss as shown in Figure 13 with an experimental attenuation of 3.75 dB per meter at 1.5 GHz, which is slightly above the theoretical level of 3.31 dB per meter. This inconsistency can be accounted for by the irregular nature of the sides of each circuit vane caused by the etching process.

The interaction impedance for this circuit is shown in Figure 14. The low values obtained are due first to the high dielectric loading by the alumina substrate, and secondly to the thick metallic conductor. The thick metallic conductor reduces the overall interaction impedance by reducing the RF fringing fields above the circuit which interact with the electron beam. Optimization of the interaction impedance and dispersion for this type of circuit could be accomplished by reducing the thickness of the metallic conductor. The dispersion would be reduced by this method by reducing the intervane capacitance. Further optimization could be achieved by utilizing a lower dielectric constant substrate material which would further decrease the effects of dielectric loading.

This circuit type could be applicable to low-cost, expendable CFA designs if tube fabrication is modified to accomodate the oxygen containing interface layers, and sole materials are selected to minimize the effects of circuit sputtering.

2. Shaped Substrate Meanderlines (SSML)

The obvious method to overcome the previously discussed limitations caused by sputtering, is to remove the intervane dielectric material. This extraneous dielectric material serves no useful electrical purpose, in fact in most cases it has a deleterious effect on the circuit characteristics evidenced by lower interaction impedance and increased dispersion (lower instantaneous bandwidth). Although the removal of the intervane dielectric material is conceptually simple, it is difficult to implement in practical applications. Manufacturers have overcome this problem by the piece part approach (see Figure 2) but at the expense of cost-reduction potential as discussed in the introduction. Figure 15 conceptually depicts the shaped-substrate meanderline circuit formed as a result of removing the dielectric material between the successive vanes, (see also Figure 16). In this program the major fabrication problems were investigated independently, while the circuit studies proceeded on the basis that a suitable fabrication technology would evolve. In the period covered by this report the fabrication technique most widely investigated was arc-plasma spraying. This process will be discussed in detail in a later section of this report. The experience gained during the CSML studies indicated that the best course of action for further circuit investigations on the shaped-substrate meanderline would be to use the microstrip theory to design experimental models. Assessment of the models would provide the appropriate reduction factors for effective dielectric constant in the shaped-substrate case. The fabrication procedures for constructing the cold-test CSML's were to a large

extent applicable to the SSML fabrication problem. The major difference was to replace the photolithographic procedure used in the CSML fabrication with a machined slotting operation to achieve the meanderline shape of the metallic conductor and substrate material simultaneously.

Three SSML circuits on polyguide dielectric were constructed on this program; two L-Band circuits which were almost identical, and one S-Band circuit.

a. L-Band Shaped Substrate Meanderline (SSML) on Polyguide Dielectric

A photograph of one of the L-Band SSML's is shown in Figure 16. The geometrical parameters for these circuits are listed in Table 4. SSML No. 2 was designed using the microstrip theory as applied to the CSML designs, however the measured characteristic impedance (Z_o) was 10 percent higher than the 50 ohm target value. A linear interpolation was used to correct the Z_o on model SSML No. 3, and measurements confirmed the drop in Z_o to the desired 50 ohm value.

The dispersion characteristics for SSML No. 2 and No. 3 are shown in Figures 17 and 18 respectively. Close examination of the dispersion curve of SSML No. 2 indicates that it is slightly larger than that of SSML No. 3. This slight variation is indicative of the characteristic impedance (Z_o) difference measured on the two models. In general, the higher characteristic impedance circuits exhibit higher dispersion caused by the corresponding decrease in the vane-to-ground plane capacitance, with the vane-to-vane capacitance remaining constant. The instantaneous bandwidth of SSML No. 2 was 1150 MHz using the $\pm$ 3 percent of c/v_p method. The instantaneous bandwidth of SSML No. 3 is slightly larger (1300 MHz) due to the slight decrease in dispersion. Both of these circuits are capable of octave bandwidth operation.

The circuit attenuation for these two models is shown in Figure 8. Both circuits exhibited similar attenuation values across the operating frequency band. SSML No. 2 had a calculated attenuation of 0.98 dB/meter at 1.5 GHz, and SSML No. 3 was slightly greater (1.08 dB/meter at 1.5 GHz) due to the small difference in characteristic impedance. The values obtained correspond closely to the theoretical value calculated at 1.5 GHz as shown in Table 5. The attenuation of the CSML is also plotted in Figure 8 and shows that attenuation of the CSML and SSML is essentially the same for identical dielectrics and value of Z_o. In Figure 9 the interaction impedance is plotted for SSML Numbers 2 and 3, and the curves overlap throughout the range of measurement. The CSML follows the same curve shape but is lower at all points in the range of interest. The improvement obtained by going to the SSML is due to the removal of the extraneous dielectric in the region between the meanderline conductors. This is the first measured confirmation of electrical performance improvement in the SSML as compared to the CSML and agrees with theoretical expectations wherein removal of dielectric material decreases the stored energy, and raises the interaction impedance.

b. S-Band SSML on Polyguide Dielectric

The encouraging results with the L-Band SSML's provided the basis for moving into S-Band. The geometrical parameters of SSML No. 4 are listed in Table 6. In the construction of this circuit a modification was made in the metal-space ratio to ease the fabrication problem. The microstrip theory was again applied along with the correction factor determined from the previous L-Band SSML experinece. A photograph of this circuit is shown in Figure 19. The OSM connectors are not attached, but the tapped holes for mounting input and output connectors can be seen. This was the first use of edge mounted connectors and it was found that coupling through the base plate is preferable for both mechanical and electrical reasons. The dispersion curve for SSML No. 4 is plotted in Figure 20, and the wide-band potential of the SSML is more apparent than was seen in the L-Band circuits. The measured attenuation at 1.5 GHz is 1.52 dB/meter, and this is in close agreement with the calculated value of 1.47 dB/meter. The variation of attenuation with frequency is shown in Figure 13. Characteristic impedance was measured and found to be 50 ohms, which is the design value. Interaction impedance of SSML No. 4 is depicted in Figure 14, and has the same shape as the L-Band SSMLs (Figure 9), but is slightly lower in value because SSML No. 4 has a lower delay ratio.

c. L-Band Arc-Plasma-Sprayed (APS) SSML on Spinel Substrate

The design concept of the cold test effort with polyguide substrates was applied to the parallel effort on circuit fabrication by use of APS. The APS approach is conceptually a low-cost technology. In this process a refractory oxide dielectric, preferably BeO , is vaporized in the intense heat of a plasma discharge and projected through a mask onto the ground plane where bonding and solidification occurs. After the build-up of the desired dielectric thickness, high purity copper is plasma sprayed onto the dielectric surface to form the metallic element of the meanderline. Conventional oxide ceramics such as alumina, magnesia, and spinel are easily sprayed in the open atmosphere. Beryllia, highly desirable because of its excellent thermal conductivity, cannot be plasma sprayed under the same conditions due to the toxic nature of this compound. Because of the special facility requirements for beryllia, the initial effort was based on a spinel (magnesium aluminate) dielectric while the beryllia spray facility was being built.[5] Microstrip theory was used to arrive at an SSML design, and the schematic depiction of this circuit is shown in Figure 21, and Figure 22 is a photograph of the completed circuit. For convenience the initial circuit was coated with gold, a nonoxidizing conductor which can be plasma sprayed in air. Table 7 lists the geometrical parameters for this circuit. The spinel as deposited had a density which was 80 percent that of the crystalline material. This porosity lowers the relative dielectric constant (ε_r) from 8.4 to 6.46 which is very close to the value for full density beryllia.

---

5. D. H. Harris, "Tailored Dielectrics," Technical Report, ECOM-0201-F, Contract No. DAAB07-73-C-0201, April 1974.

An equivalent porosity in beryllia would negate to a large extent the excellent heat transfer properties of this material, and for this reason the APS effort was later directed towards formation of high density ceramic deposits. Another problem with porosity is the attendant roughness of the dielectric surface on the ground plane and beneath the deposited metallic meanderline. The attenuation of the APS circuit is shown in Figure 8, and is higher than expected from theoretical considerations (see Table 5). The cause of this problem was not immediately apparent but an explanation was eventually found by measuring the dc resistivity of the gold overlay. Based on a reported gold thickness of 0.05 mm it was determined that the sprayed metal had a resistivity 4.5 times greater than the bulk metal value. Taking this into consideration the high frequency loss would be raised to a calculated value of 2.55 dB/meter. This does not account for all of the unexplained loss but surface roughness and/or a thinner gold layer than reported would explain the difference. The phase-frequency relationship of the APS circuit is plotted in Figure 23. The mid-band delay factor of 17.5 is typical of that used in many crossed-field amplifiers. Figure 14 shows interaction impedance of the APS circuit. Dielectric loading and a lower characteristic impedance caused a substantial reduction in interaction impedance from that realized with the polyguide supported circuits.

d. Northrop L-Band Simulated SSML on Stycast 6

The encouraging performance of SSMLs in cold test and problems arising in fabrication of circuits adequate for hot tests made it advisable to obtain tube-operational data even though low-cost circuits would not be available for some time. This approach was implemented by an external contract in which a firm with production experience in CFA's using shielded meanderlines was funded to test a simulated SSML in a hot tube. This simulation consisted of fabricating the dielectric substrate from discrete pieces, setting the individual parts into a grooved ground plane, and overlaying the assembly with a copper meanderline made by current production methods. Figure 24 depicts the concept, and the photographs in Figures 25, and 26 are a top and a side view respectively of the L-Band SSML fabricated from dielectric segments. Simulation was necessary because of the non-availability of a one piece ceramic shaped-substrate. Furthermore, in an operating tube, there would be an additional fabrication problem because of differential thermal expansion between the ceramic and the copper ground plane. This difficulty will be solved in the future by means of a coexpansive ground plane. Table 8 lists the geometrical parameters for this circuit. Figure 9 is the interaction impedance of an L-Band cold test circuit built by Northrop. The interaction impedance is lower than the circuits with polyguide dielectric because of the higher dielectric constant substrate in the Northrop circuit. The change in curve shape at the lower frequencies is caused by grooving of the ground plane, embedding of the dielectric, and also by the thicker metal of the meanderline circuit. The results gave a high degree of confidence that an S-Band CFA could be built utilizing a simulated SSML scaled from the L-Band cold test circuit, and this task was subsequently pursued by the contractor. Figure 27 shows the dispersion for the L-Band simulated SSML cold test circuit. The mid-band phase delay of 18.3 was considered excellent for the selected beam operating potential. The dispersion was somewhat higher than anticipated, and was

caused by the thick metallic conductor, and the grooving of the ground plane assembly. The experimental results indicate an instantaneous bandwidth of approximately 500 MHz centered at 1.5 GHz. Actual circuit attenuation measurements were not conducted because the circuit delivered by the contractor had only one RF connector. However, the calculated circuit attenuation was 1.73 dB/meter and is shown in Table 5.

e. Northrop S-Band Hot Test Results for Simulated SSML on Beryllia Dielectric

The successful L-Band simulated SSML was scaled into S-Band by multiplying all dimensions by a scaling factor of approximately 0.6. This value is not exact since the small dielectric constant difference between Stycast HiK6 (ε_r= 6.0) used in the L-Band circuit and beryllia (ε_r = 6.6) required in the hot tube must be taken into account. Table 9 lists the geometrical parameters of the resultant S-Band design. The simulated SSML anode circuit was fabricated and assembled using procedures essentially the same as those used in production tubes. The simulated SSML anode circuit was then mounted in a standard production CFA body in place of the shielded meanderline.[6] The substitution method was used to demonstrate the hot test characteristics of the simulated SSML, so that fabrication and assembly costs could be held to a minimum by utilizing standard production line piece parts.

Figure 28 is a photograph of the S-Band injected-beam CFA (IBCFA) which contains the simulated SSML circuit. The package configuration including the magnetic structure is comparable to the Northrop S-Band IBCFA production model.

Representative hot test performance is listed in Table 10. Maximum power output for this device was 3.1 kW across an instantaneous 1 GHz frequency band (2.5-3.5 GHz).The hot test instantaneous bandwidth performance of 1/2 octave was expected, since the L-Band cold test model exhibited similar dispersion. The total frequency range was 2.0 to 4.0 GHz with three different sole potentials to optimize the power output across the one octave band. Duty was held at 10 percent maximum to characterize the device at low average power, avoiding the risk of circuit destruction due to excessive dissipation and/or arcs. The liquid-cooled anode circuit structure is capable of dissipating in excess of 2 kW of average power.

The maximum demonstrated gain was 19 dB, and the efficiency neglecting drive power was 30 percent. These values are equivalent to the S-Band production model.

Although the tube was not optimized for the SSML circuit design, the hot test performance was equivalent to or better than the S-Band production line device with a shielded meanderline. The hot test phase of this effort did attain the intended objective of demonstrating the capabilities and simplicity of the simulated shaped-substrate meanderline in an operating IBCFA. Based on these excellent results better performance is expected by utilizing a one piece shaped-substrate meanderline anode structure on a flat ground plane.

---

6. R. R. Moats, "Low-Cost Crossed-Field Amplifier," Technical Report, ECOM-75-1343-F, Contract No. DAAB07-75-C-1343, June 1977.

CONCLUSIONS

The internal ERADCOM effort has shown that the shaped-substrate meanderline anode circuit is a viable concept for obtaining high-performance, octave-bandwidth, injected-beam CFA's, and is being applied to moderate-power CFA development efforts.

Hot tests of the simulated SSML confirmed the theory previously developed during the ERADCOM cold test investigations. Furthermore, the practicality of the SSML was established, and its performance was comparable to the complex shielded meanderline used in current production line models. The substitution technique used in the hot test phase is a highly desirable method since there is a significant reduction in both overall expense, and time required to demonstrate new design concepts where applicable.

The original CSML cold test effort has provided the basis for continued efforts related to the development of low-cost expendable jammers for electronic warfare application. If the sputtering problems inherent in the typical CSML device can be overcome, this circuit type would be considered an excellent candidate for the short-life application.

The fabrication procedures for achieving an ultimately low-cost, one-piece substrate did not evolve to a practical level during this phase of the ERADCOM internal effort. The arc-plasma-spray process was considered conceptually ideal for obtaining low-cost circuits, however, the contractual effort did not yield useful circuits because of difficulties in depositing high-density ceramic substrates and low-resistivity conductive layers. For this reason the technology phase of the internal effort was redirected to pursue an alternate fabrication method.

A precision laser machining fabrication process was selected as the most adaptable technique for fulfilling the electrical and mechanical requirements of the SSML. As a result of recent internal and contractual investigations, the laser-cutting process has demonstrated the potential for achieving broadband, moderate-power, CFA anode circuits while meeting the low-cost objective of this program. Northrop Corporation is presently under contract (DAAB07-77-C-2642) to develop crossed-field amplifiers utilizing this new fabrication approach at 2-4 GHz, and 8-18 GHz. The results of the internal and contractual efforts pertaining to the laser-cutting approach will be consolidated into a separate report.

An assessment of all the low-cost fabrication approaches indicates that the co-expansive ground plane is an absolute requirement for constructing circuits with a one-piece ceramic substrate to avoid substrate fracture during bonding. Contractual efforts are underway at Northrop Corporation (contract No. DAAB07-77-C-2642) to investigate the use of composite, co-expansive materials (tungsten-copper), associated bonding processes, and methods for incorporating these assemblies into actual hot-test tubes.

Scaling the basic SSML design to higher and lower frequencies is feasible, however, in order to avoid over-miniaturization encountered at high frequencies (>15 GHz) requires the use of substrate materials having dielectric constants lower than beryllia. Boron nitride and diamond substrates are possible candidates for the high frequency applications.

Cost, thermal conductivity, and dielectric constant trade-off investigations should be conducted to formulate practical, high-frequency SSML anode designs.

The direct-bonded-copper metallization technique exhibited difficulties concerning bonding voids which were considered a serious drawback to producing high-power CFA circuits. This metallization process is only applicable to oxide based ceramics such as alumina and beryllia. Recent improvements in this technique have resulted in bonding interface layers exhibiting excellent thermal conductivity and low RF loss. These improvements, along with the use of applicable ceramic substrates, will make this process attractive for future microwave tube development efforts.

REFERENCES

1. H. L. Mc Dowell, "Ceramic Mounted Circuit for Crossed Field Amplifiers," Technical Report ECOM-0273-F, Contract No. DAAB07-72-C-0273, March 1974.

2. P. N. Hess, H. Kohlmoos, Jr., "Study of Interaction Structures," Technical Report ASD-TDR-62-813, Contract No. AF 33(616)-8078, Nov. 1963.

3. M. Caulton, et al., "Measurements on the Properties of Microstrip Transmission Lines for Microwave Integrated Circuits," RCA Review, Vol. 27, No. 3, Sep. 1966.

4. Y. S. Sun, J. C. Driscoll, "A New Hybrid Power Technique Utilizing a Direct Copper to Ceramic Bond," IEEE Trans. Electron Devices, Vol. ED-23, No. 8, pp. 961-967, August 1976.

5. D. H. Harris, "Tailored Dielectrics," Technical Report ECOM-0201-F, Contract No. DAAB07-73-C-0201, Apr. 1974.

6. R. R. Moats, "Low-Cost Crossed-Field Amplifier," Technical Report ECOM 75-1343-F, Contract No. DAAB07-75-C-1343, June 1977.

BIBLIOGRAPHY

1. S. Ramo, J. Whinnery, & T. Van Duzer, Fields and Waves in Communication Electronics, John Wiley & Sons, Inc., New York, New York, 1965.

2. J. D. Kraus, Electromagnetics, McGraw-Hill, New York, New York, 1953.

3. W. C. Johnson, Transmission Lines and Networks, McGraw-Hill, New York, New York, 1950.

4. R. J. McCormack, S.S. Sussman, "Interaction Impedance Calculations, Techniques, and Examples," Technical Memorandum, Job 99-11, (SFD Laboratories, Inc.), 1966.

5. M. Ettenberg, "Planar Circuits for Microwave Tubes," Progress Report No. 1, US Army Research Office - Durham, Contract No. DAHC04-74-G-0214, Mar. 75.

6. J. F. Burgess, and C. A. Neugebauer, US Patent No. 3,911.553, Oct 1975.

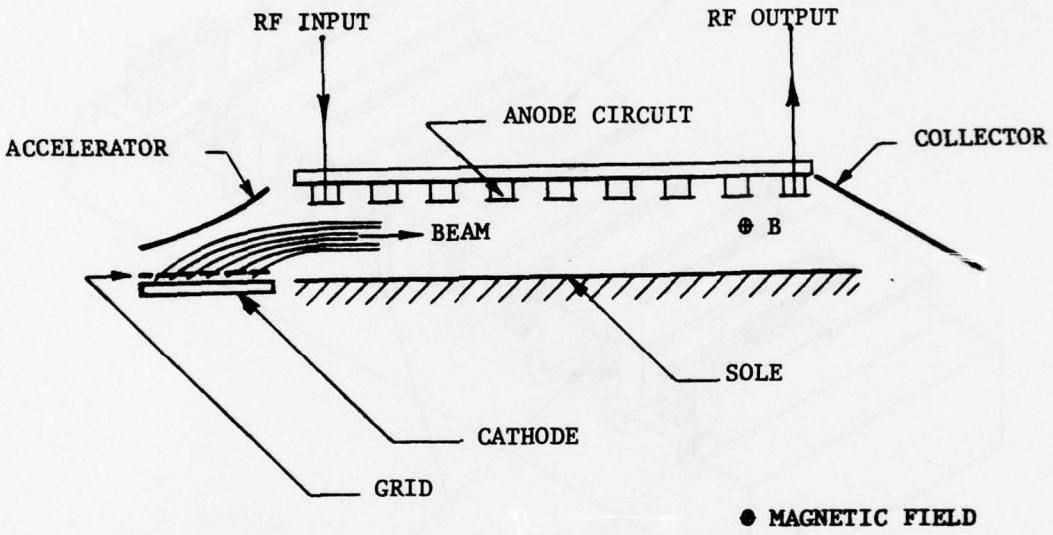

Figure 1. Configuration of Typical Linear-Format, Medium-Power Crossed-Field Amplifier (CFA)

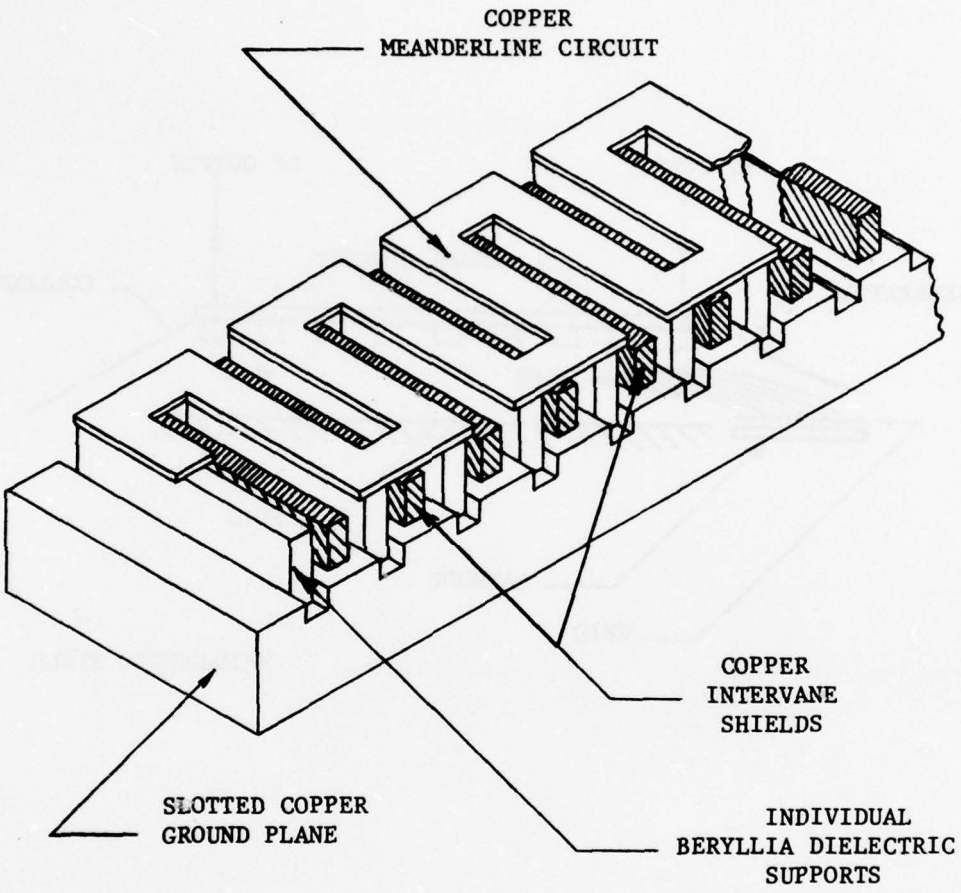

Figure 2. Typical Shielded Meanderline Anode Circuit on Ground Plane

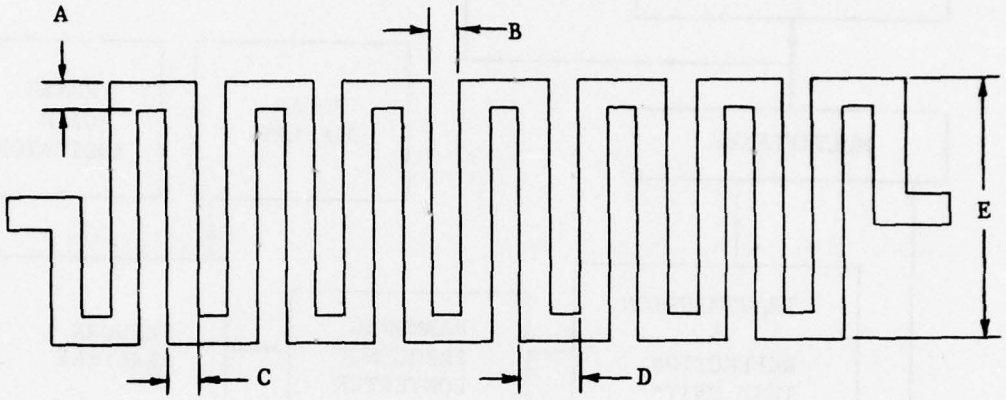

A - ADVANCE WIDTH

B - SLOT OR GAP WIDTH

C - VANE WIDTH

D - CIRCUIT PITCH

E - CIRCUIT HEIGHT

$\frac{C}{B}$ - VANE-TO-SLOT RATIO OR METAL-TO-SPACE RATIO

Figure 3. Basic Meanderline Configuration and Definitions

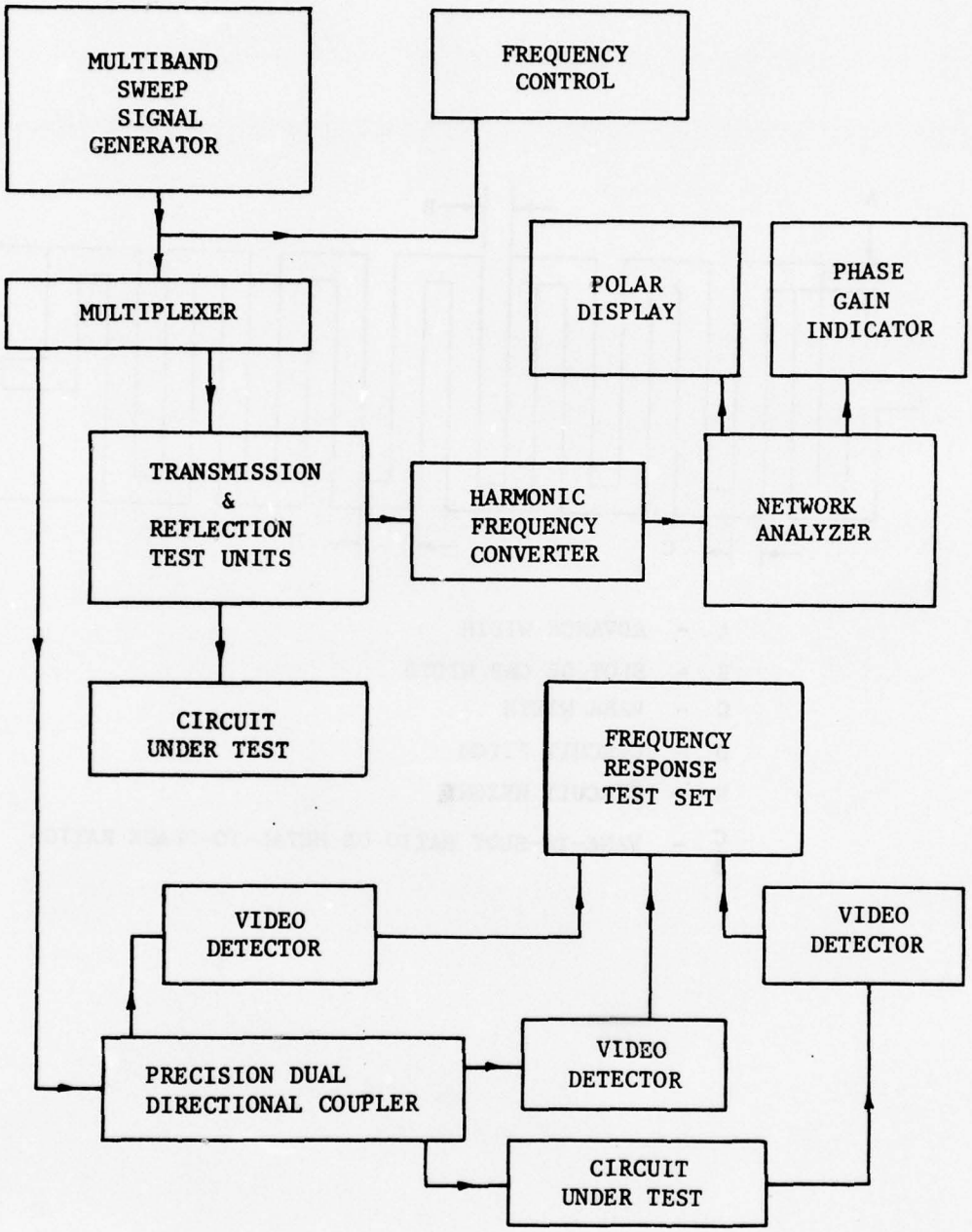

Figure 4. Equipment Block Diagram

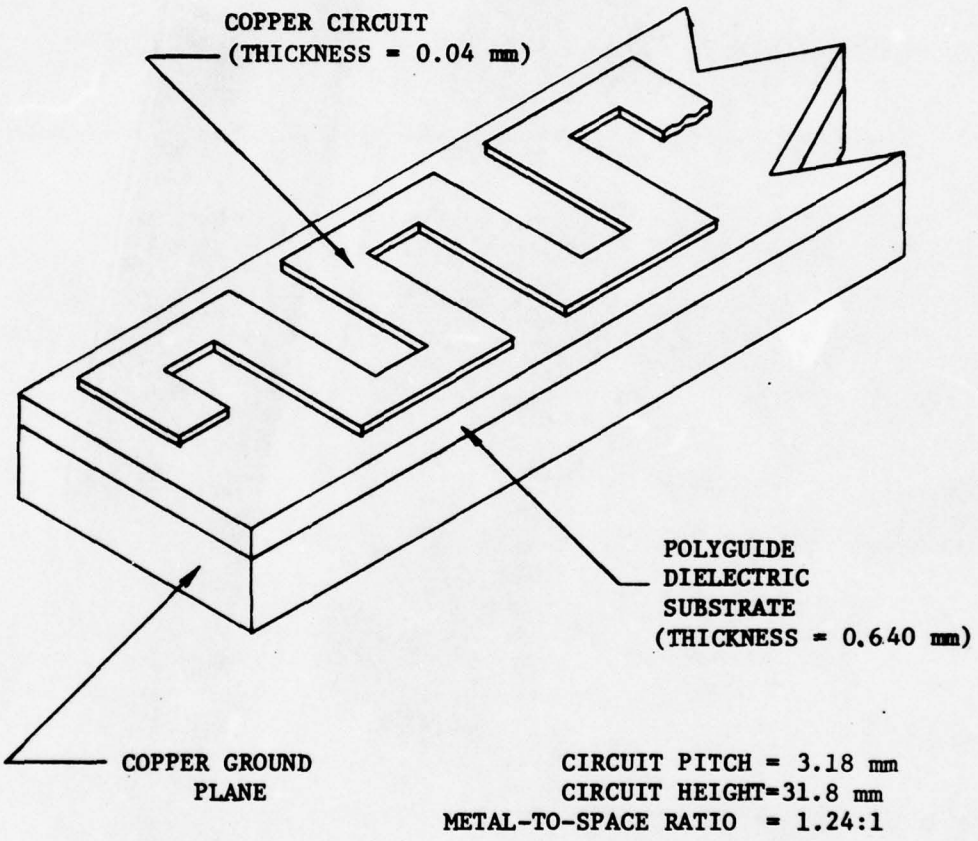

Figure 5. Continuous Substrate Meanderline (CSML) Configuration

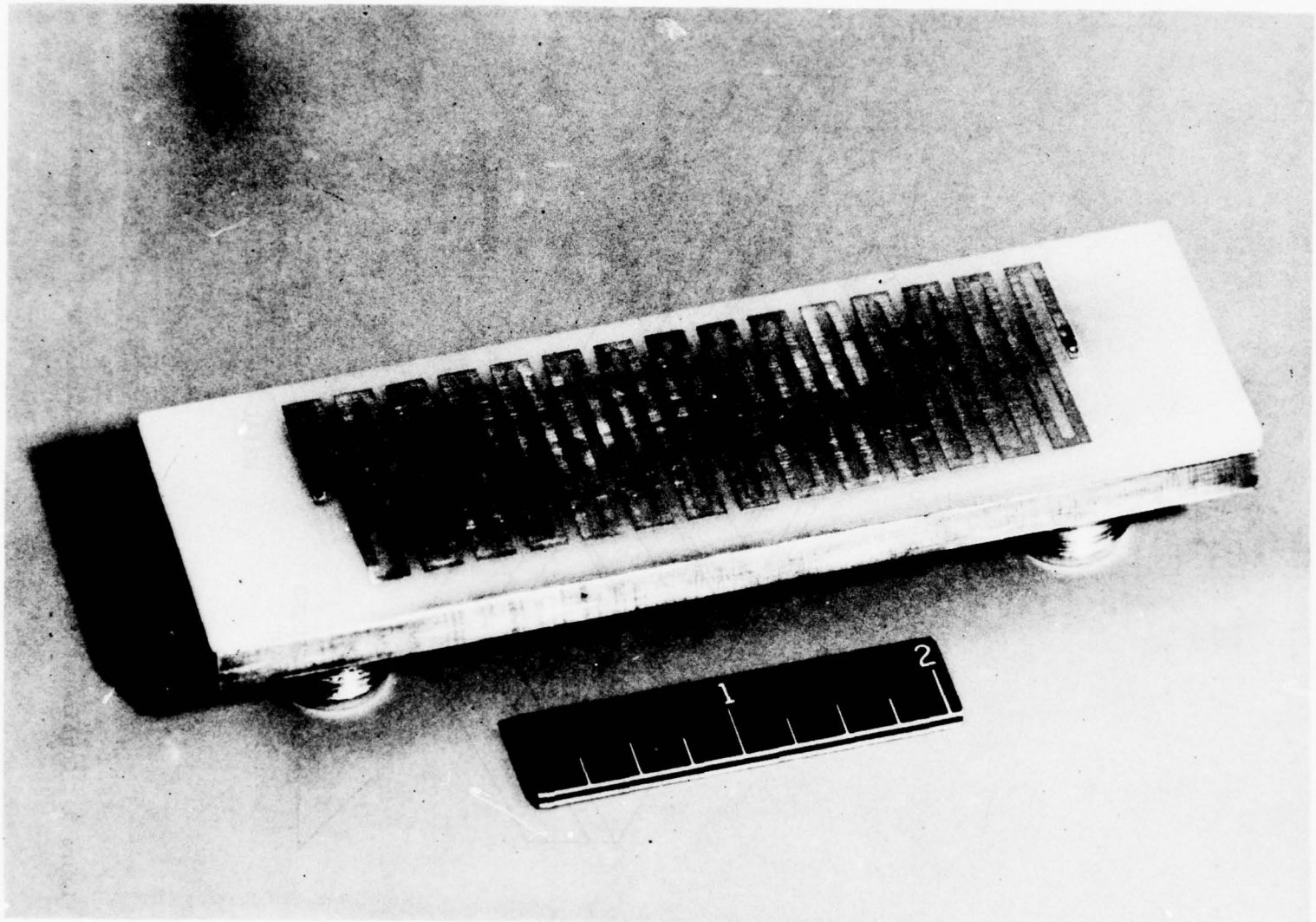

Figure 6. Continuous Substrate Meanderline (CSML) on Polyguide Dielectric

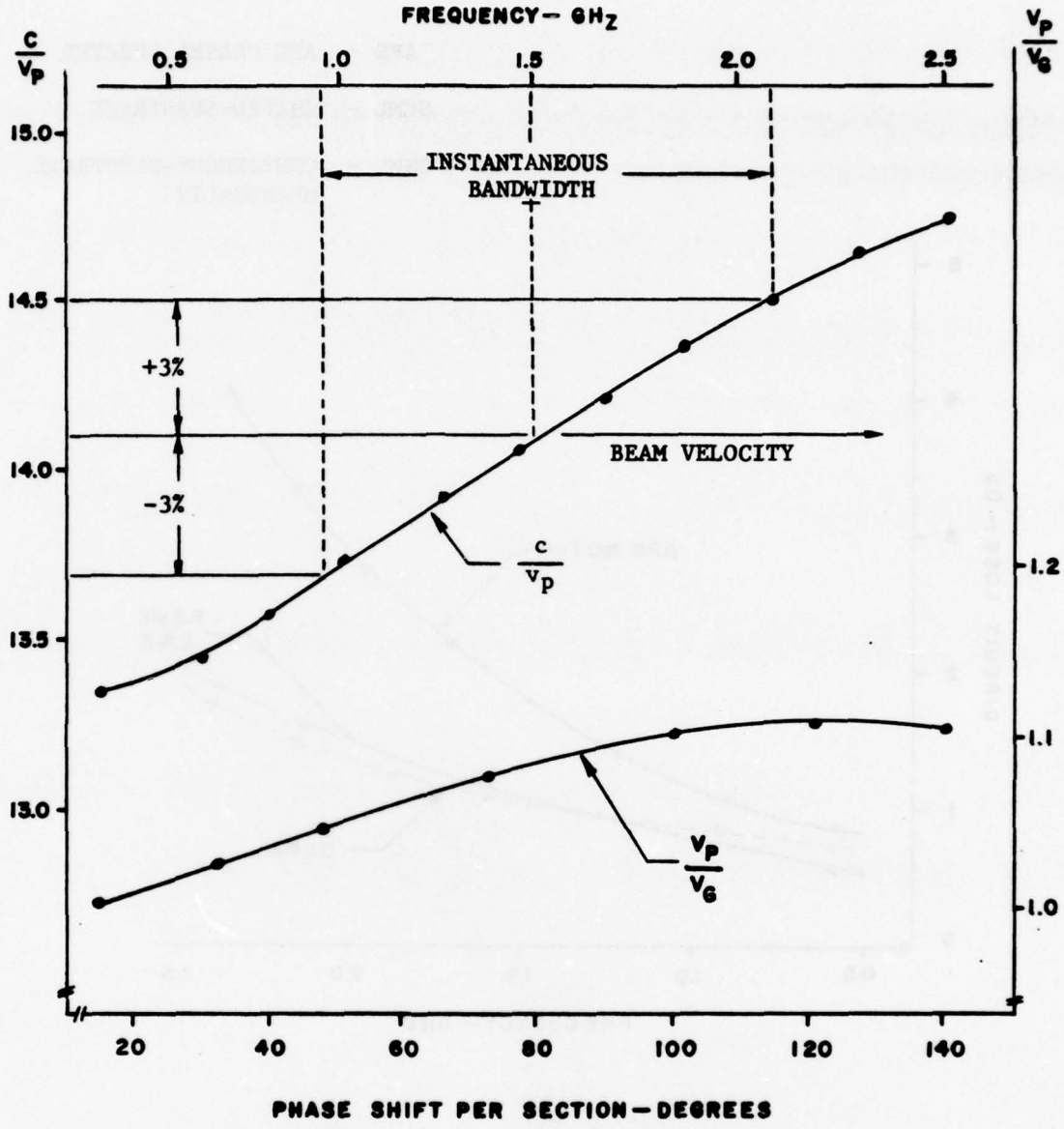

Figure 7. Dispersion Curves for L-Band Continuous Substrate Meanderline on Polyguide Dielectric

APS - ARC PLASMA SPRAYED

SCML - SHAPED-SUBSTRATE

CSML - CONTINUOUS-SUBSTRATE MEANDERLINE

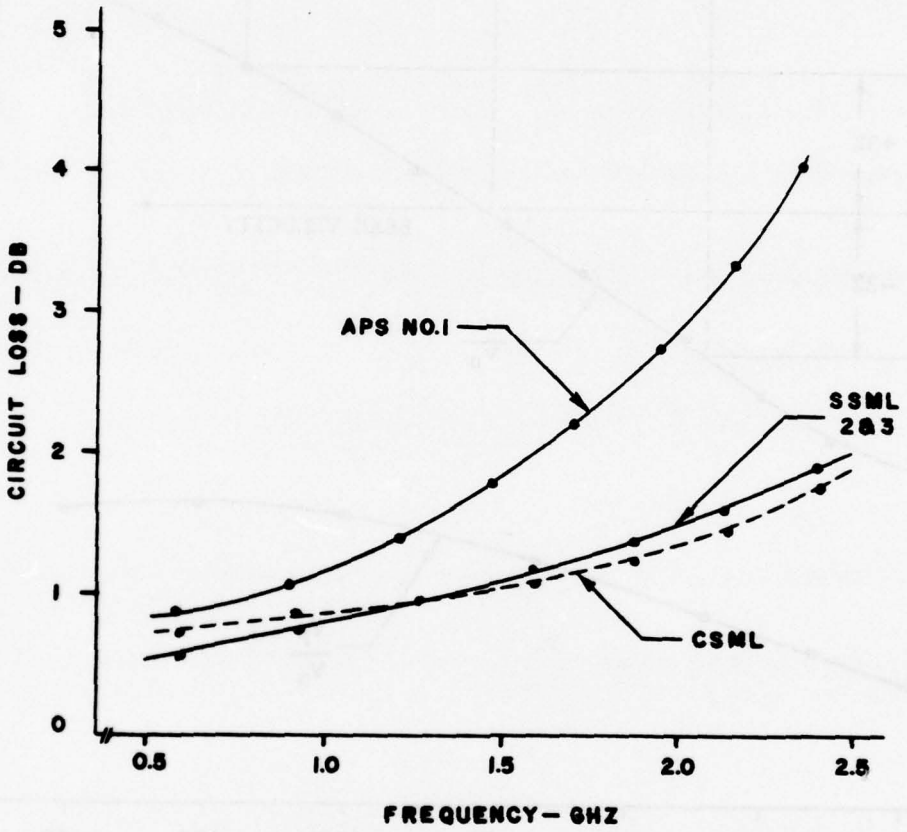

Figure 8. Circuit Loss Vs Frequency for L-Band Arc-Plasma-Sprayed (APS) Shaped Substrate Meanderline (SSML), L-Band SSML's Nos. 2 and 3, and L-Band CSML

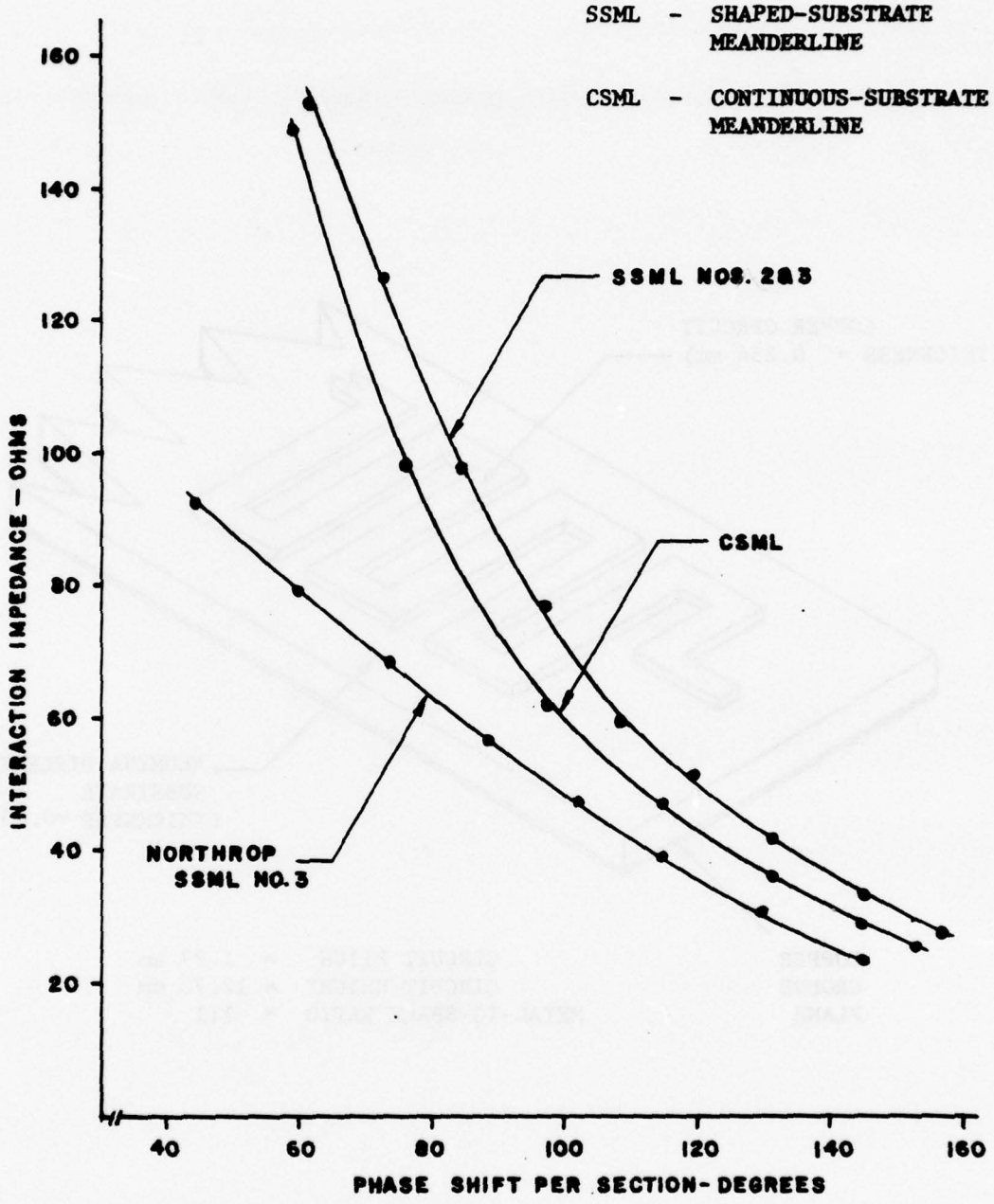

Figure 9. Interaction Impedance Vs Phase Shift Per Section for L-Band SSML's Nos. 2 and 3, L-Band CSML, and Northrop L-Band SSML No. 3

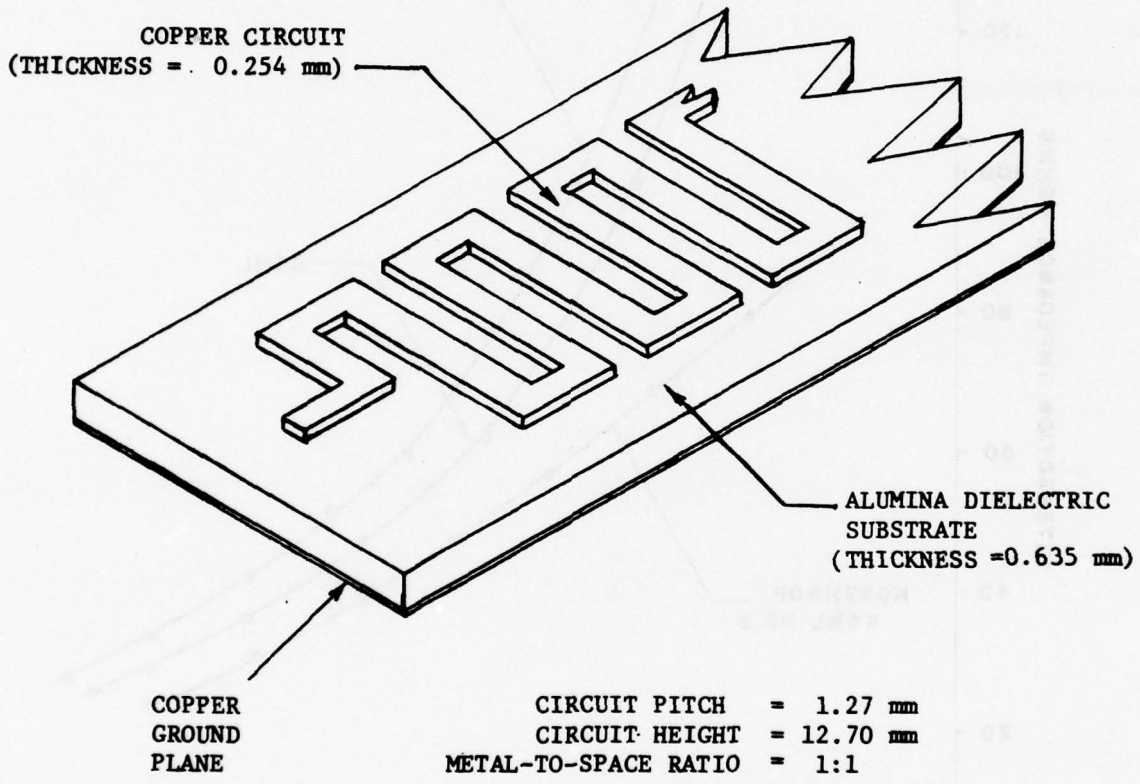

Figure 10. Direct-Bonded-Copper (DBC) S-Band CSML Circuit Configuration

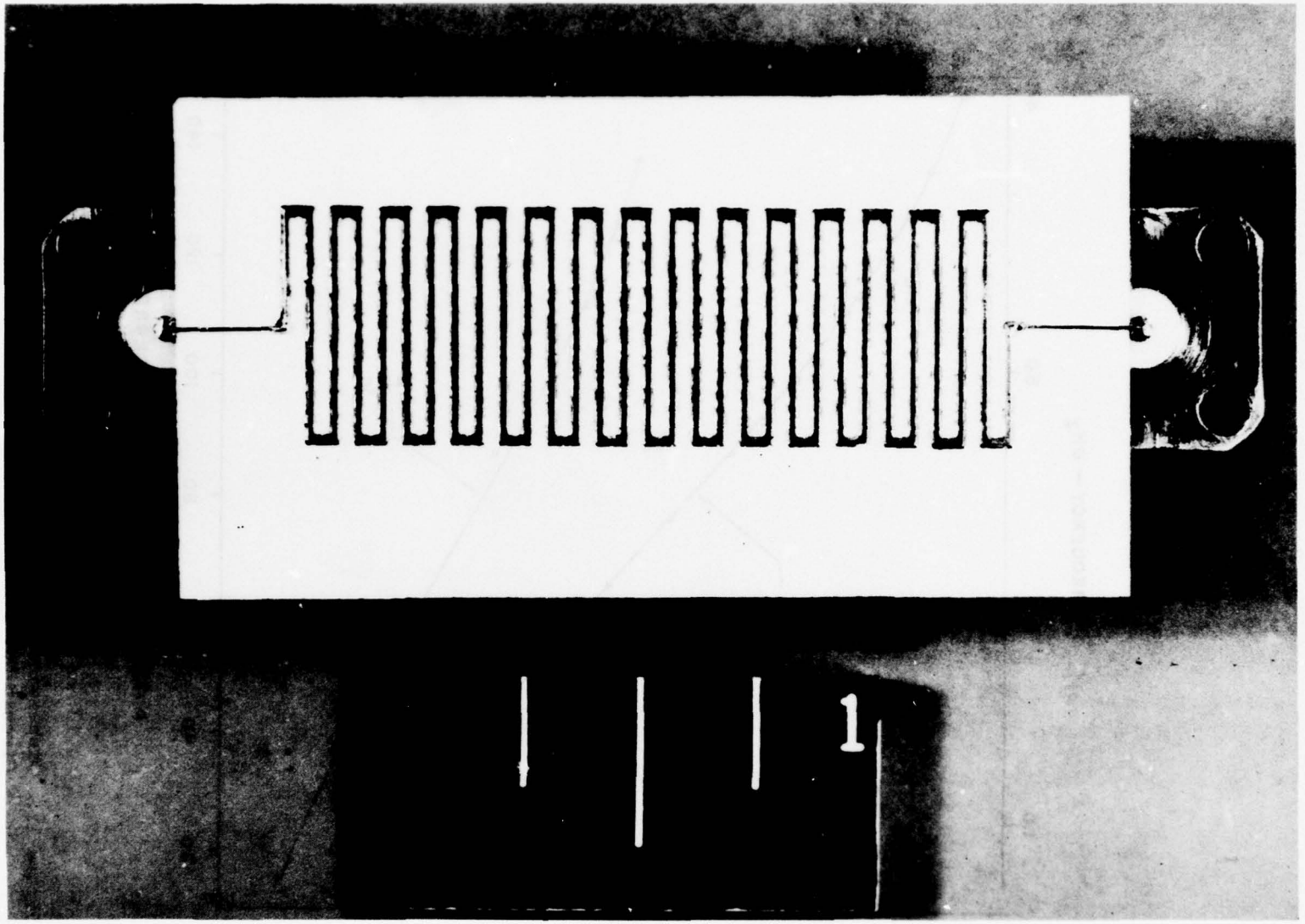

Figure 11. S-Band DBC Circuit on Alumina

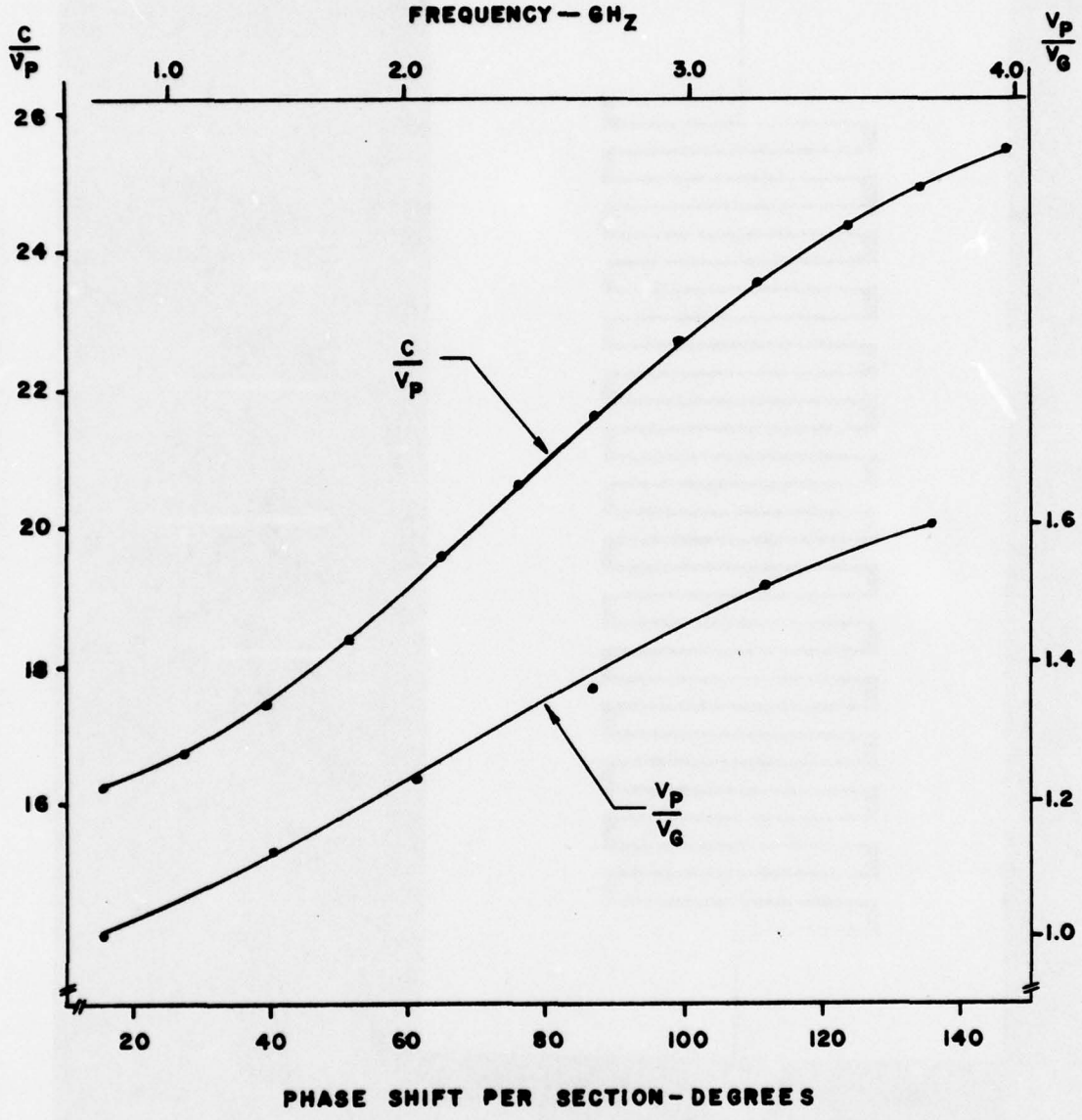

Figure 12. Dispersion Curves for CSML Direct-Bonded-Copper (DBC) Circuit No. 1

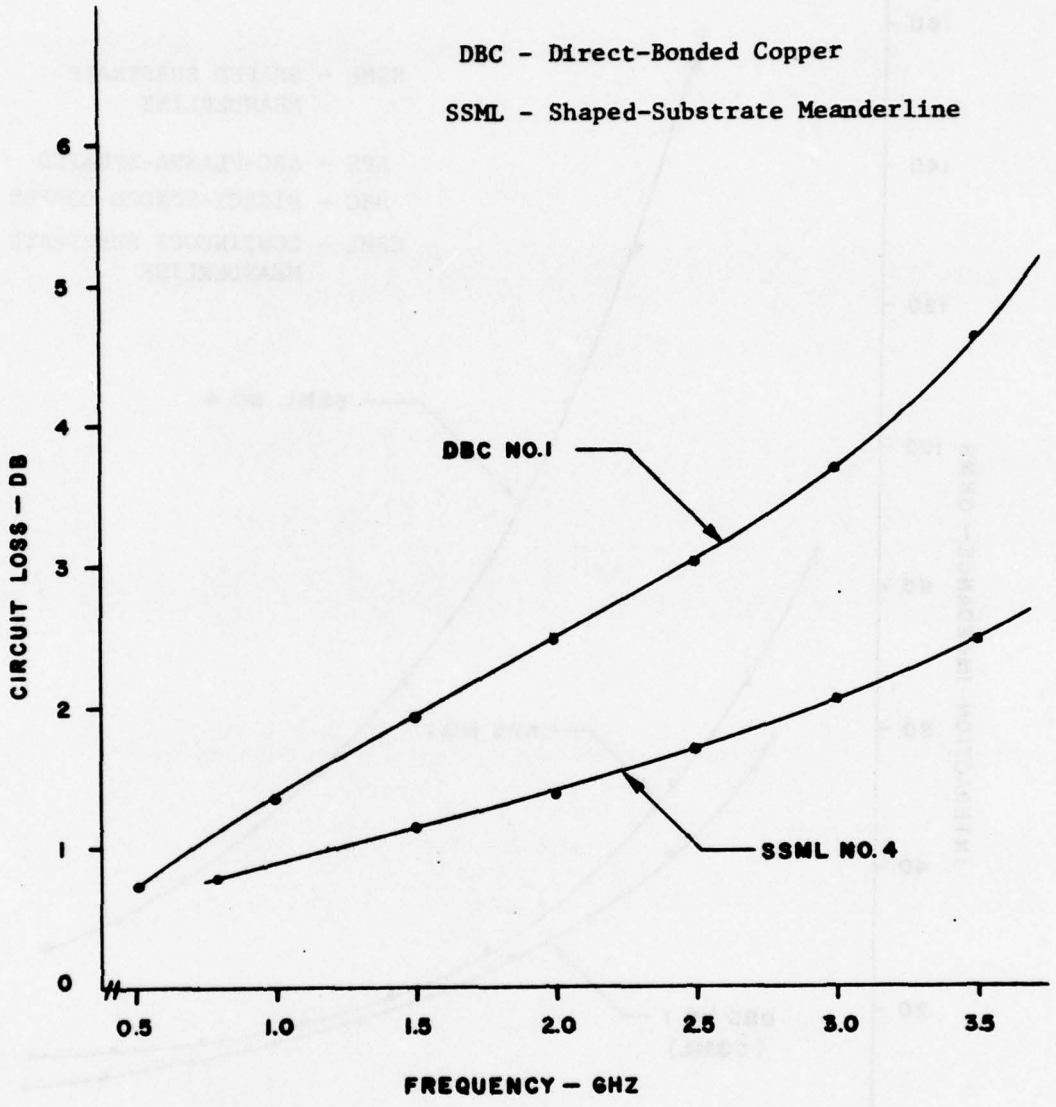

Figure 13. Circuit Loss Vs Frequency for DBC No. 1 and SSML No. 4

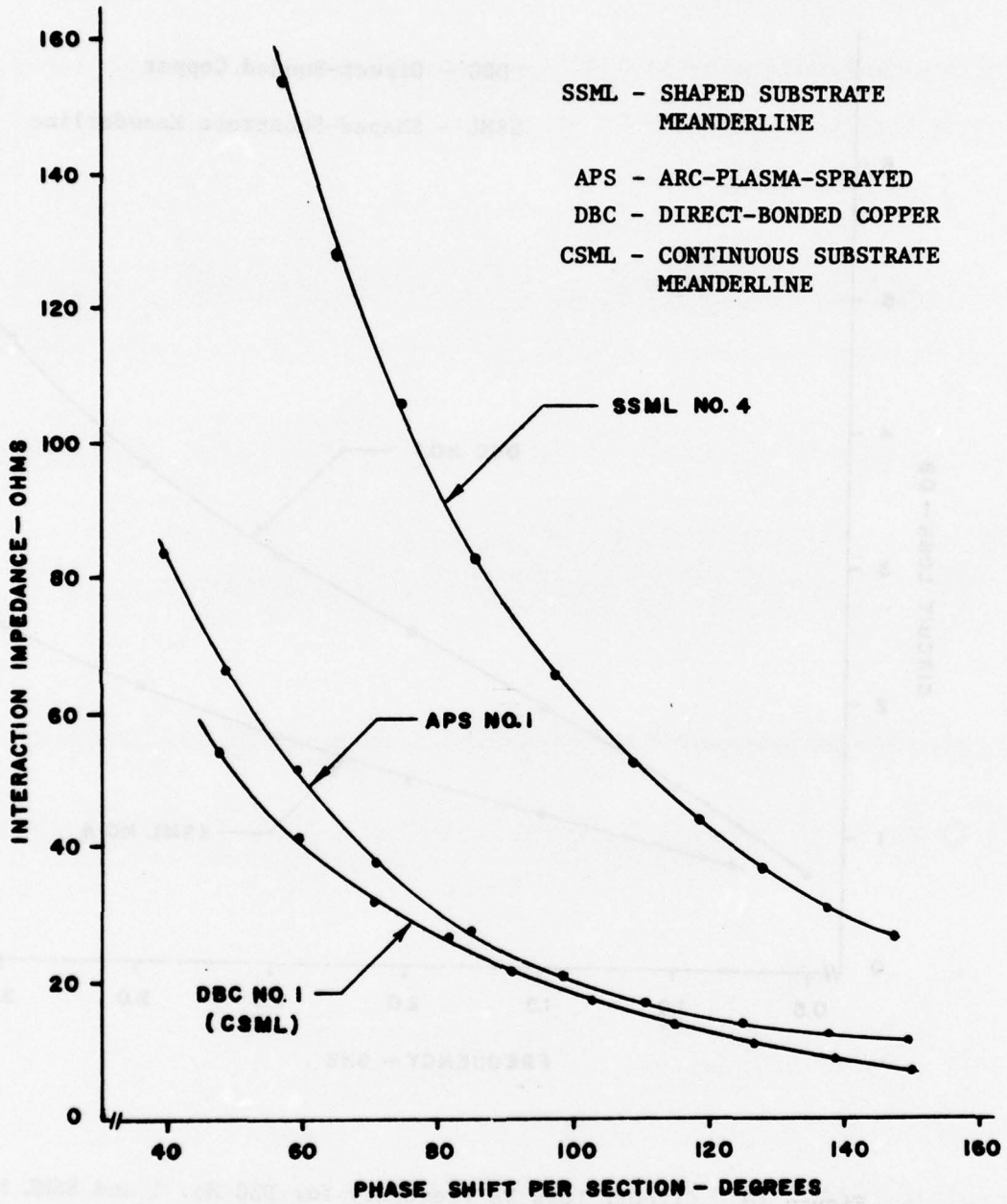

Figure 14. Interaction Impedance Vs Phase Shift Per Section for DBC No. 1, SSML No. 4, APS No. 1

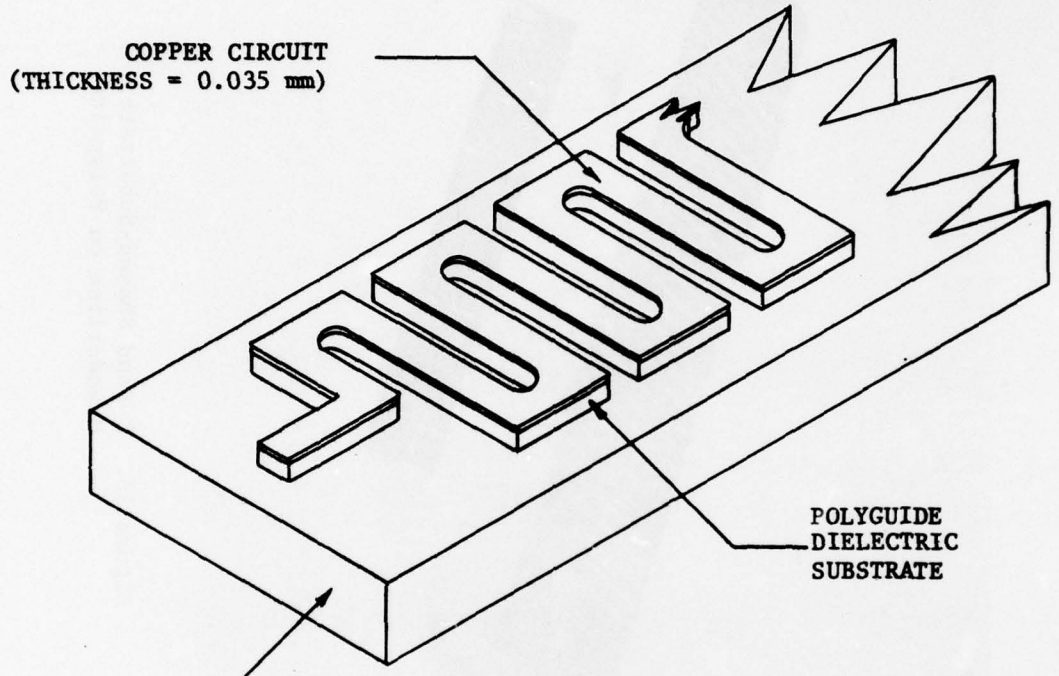

	SSML #2 L-BAND	SSML #4 S-BAND
CIRCUIT PITCH	= 3.18 mm	2.54 mm
CIRCUIT HEIGHT	= 32.0 mm	21.34 mm
METAL-TO-SPACE RATIO	= 1.0:1	1.13:1
SUBSTRATE THICKNESS	= 0.574 mm	0.422 mm

Figure 15. Shaped-Substrate Meanderline on Ground Plane Configuration

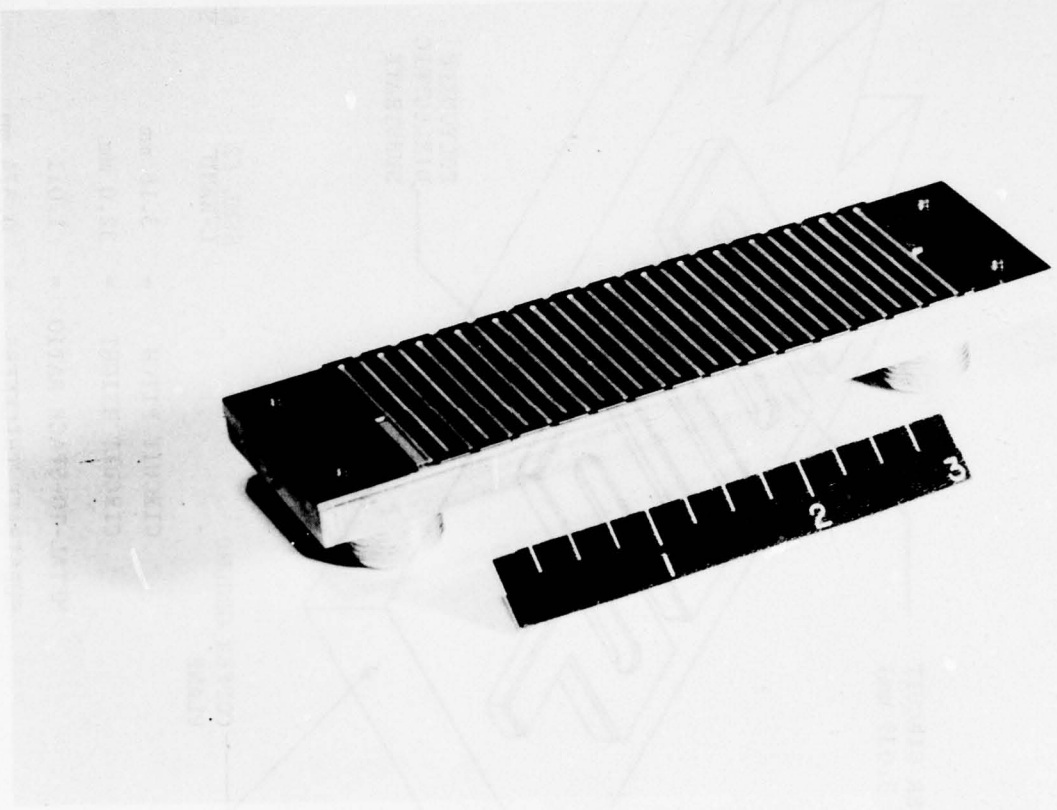

Figure 16. L-Band Shaped-Substrate Meanderline on Polyguide

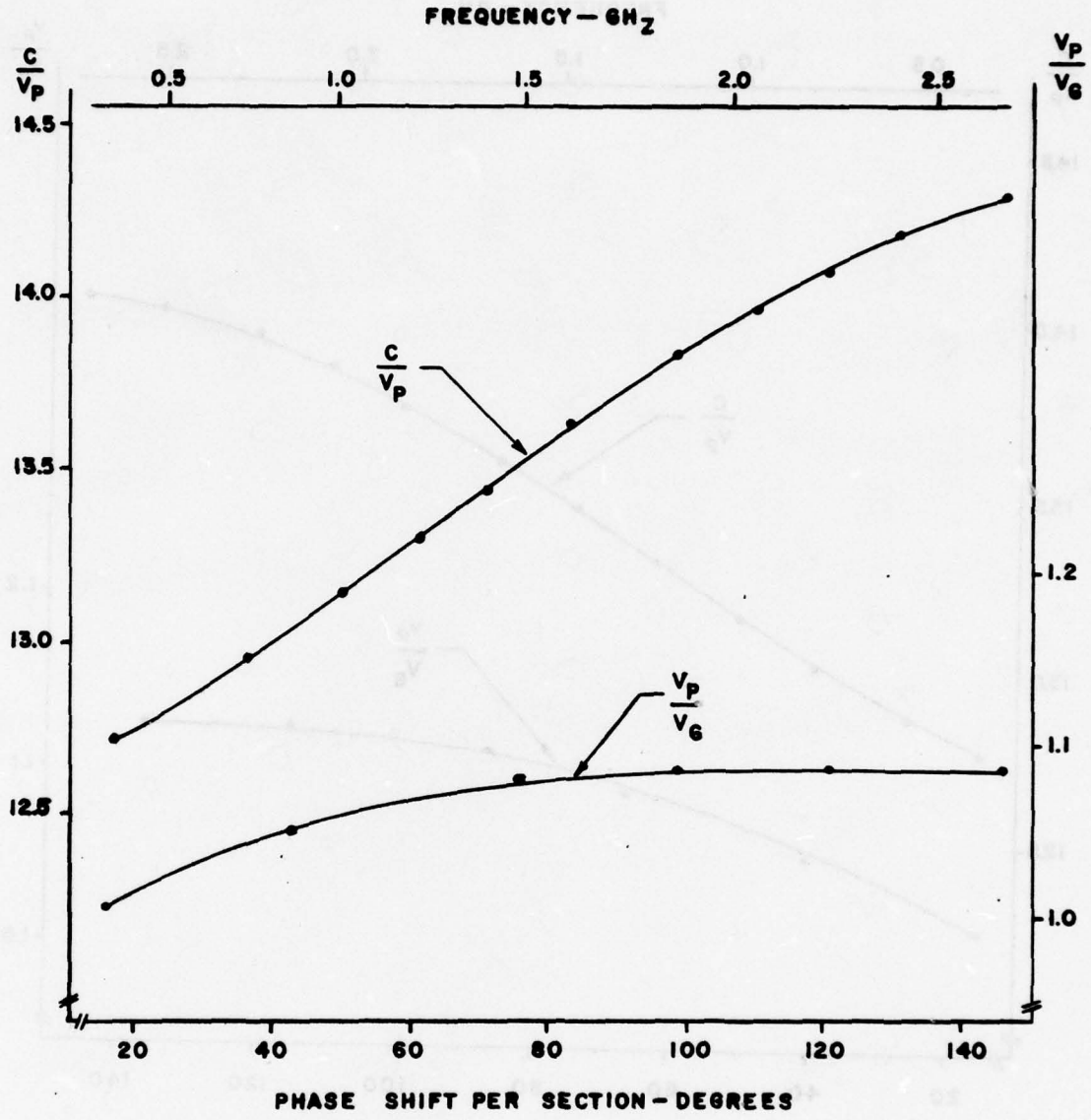

Figure 17. Dispersion Curves for L-Band SSML No. 2

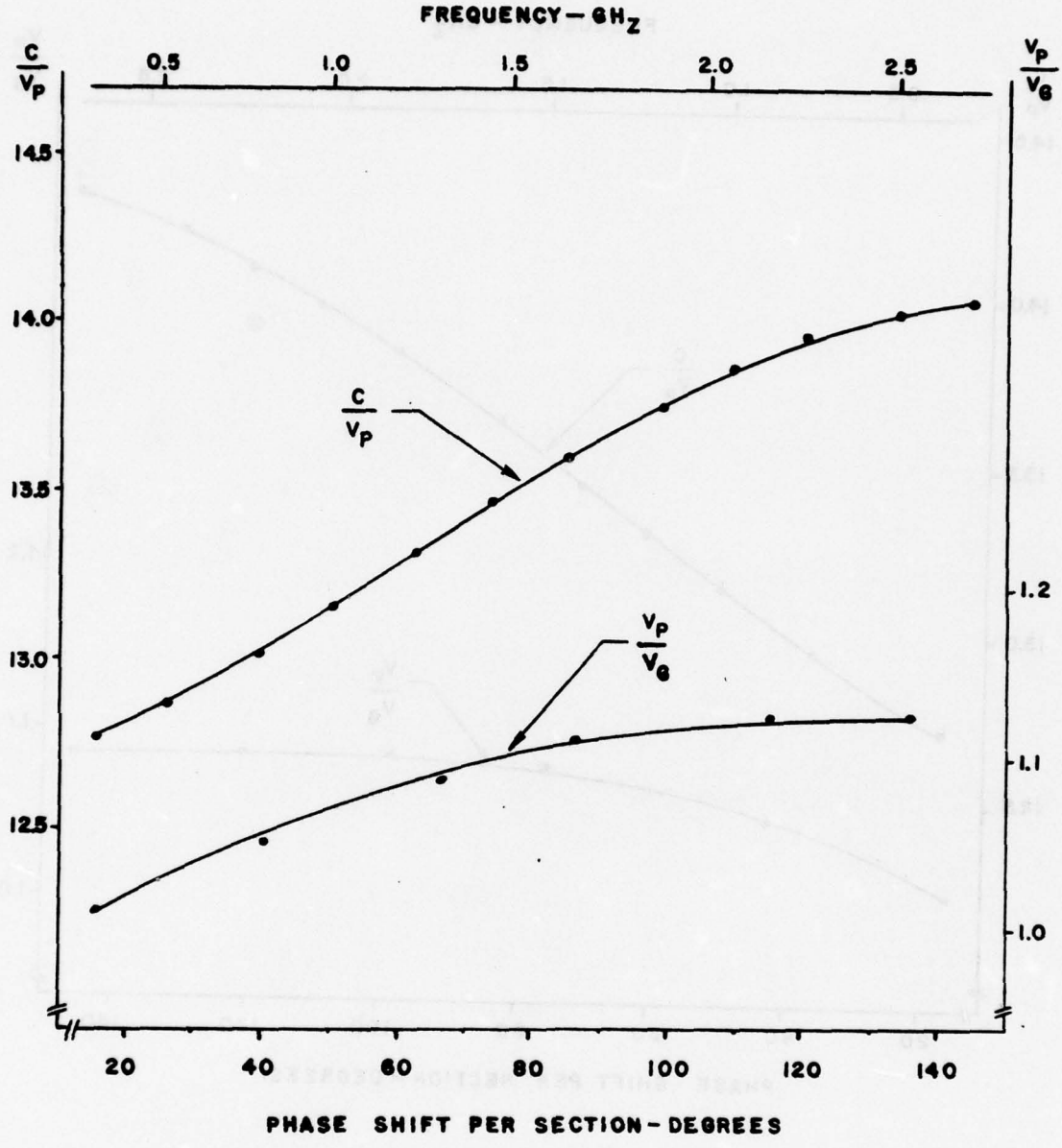

Figure 18. Dispersion Curves for L-Band SSML No. 3

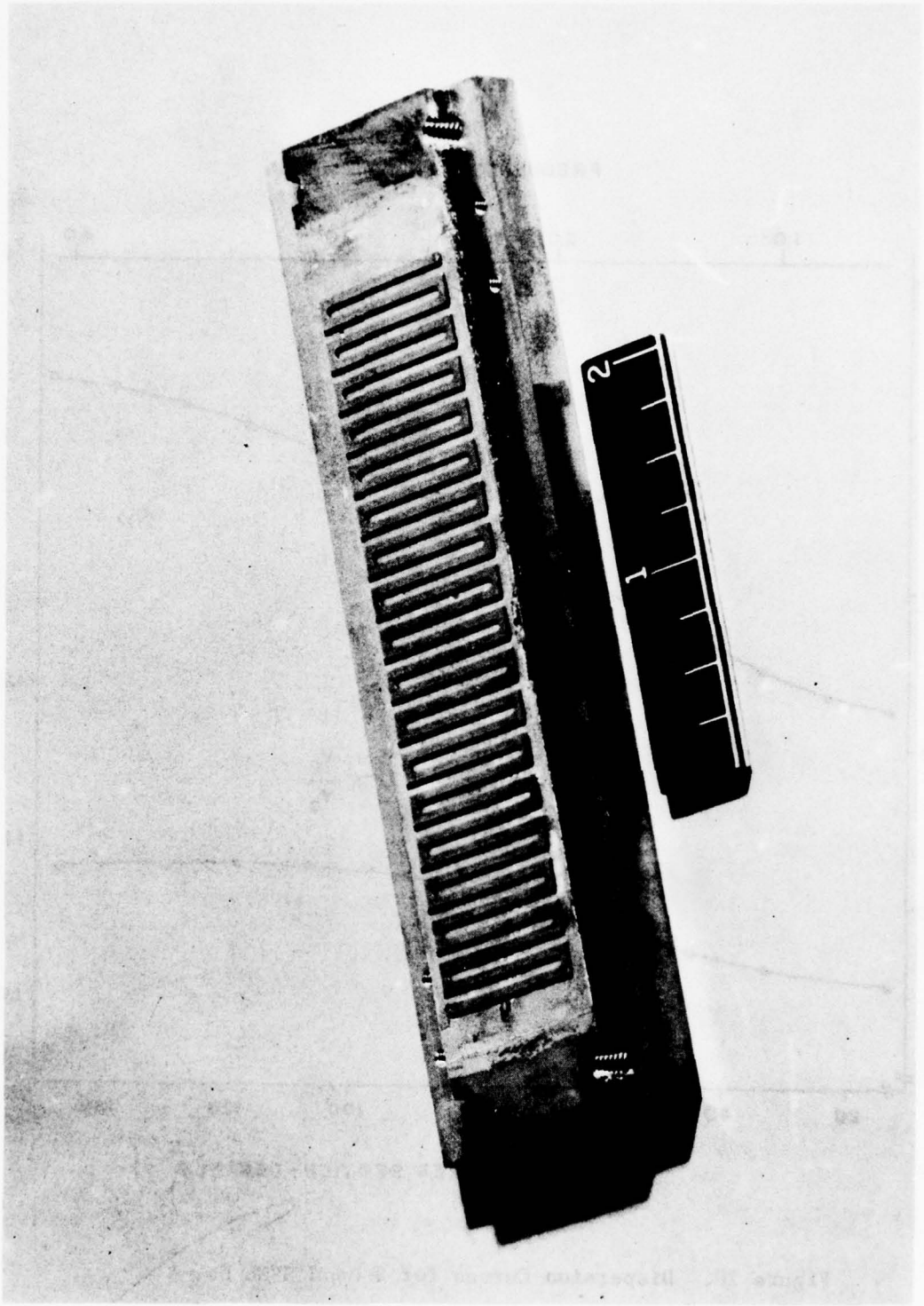

Figure 19. S-Band SSML No. 4 on Polyguide

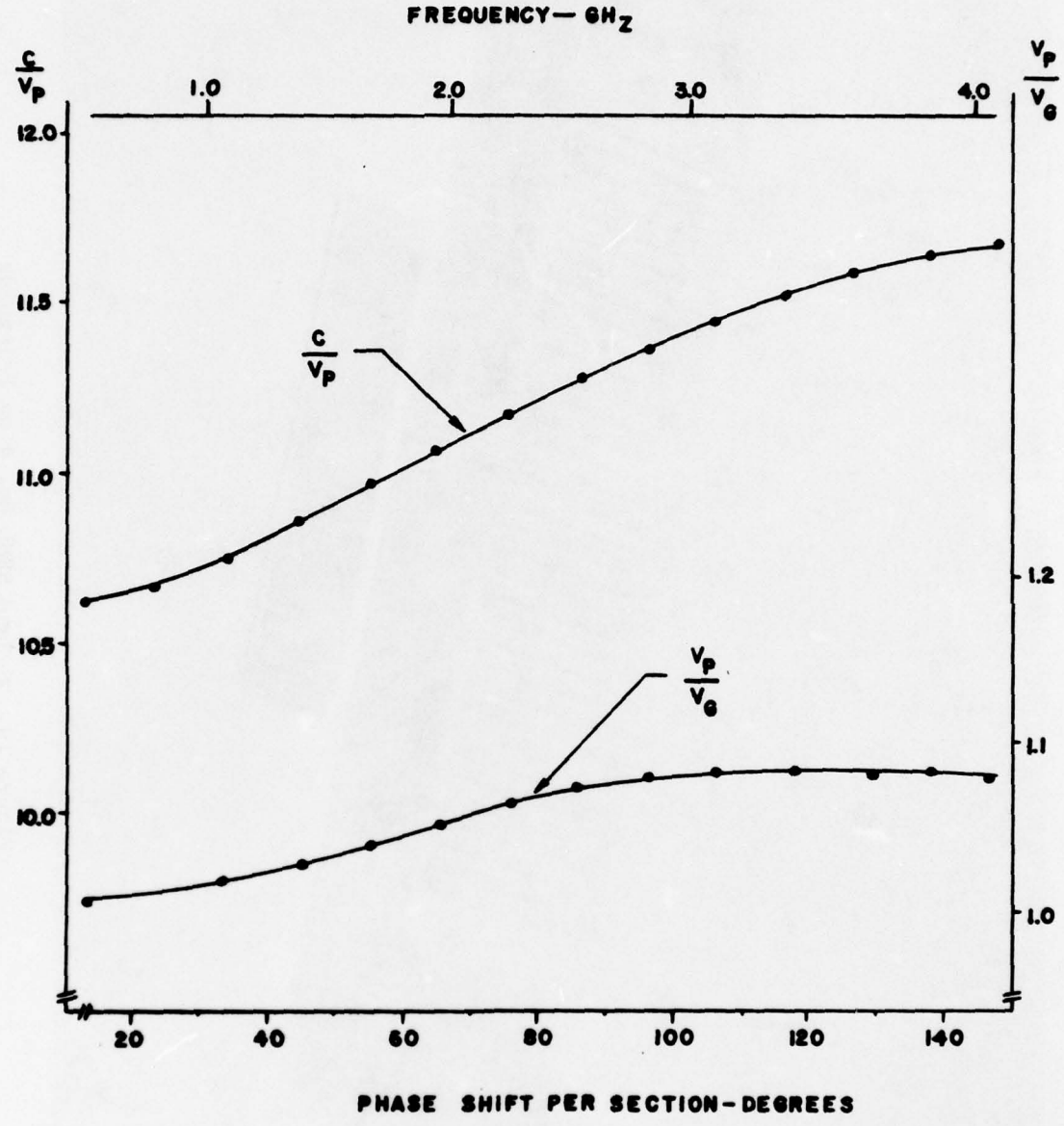

Figure 20. Dispersion Curves for S-Band SSML No. 4

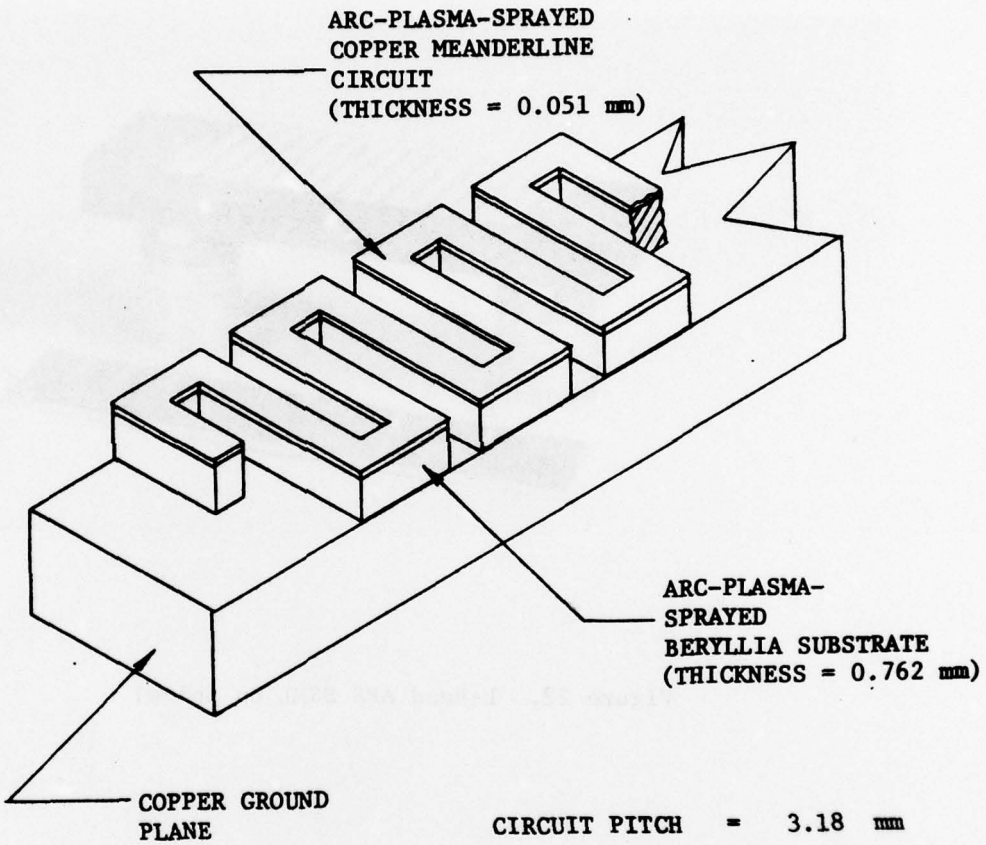

Figure 21. APS Meanderline Configuration

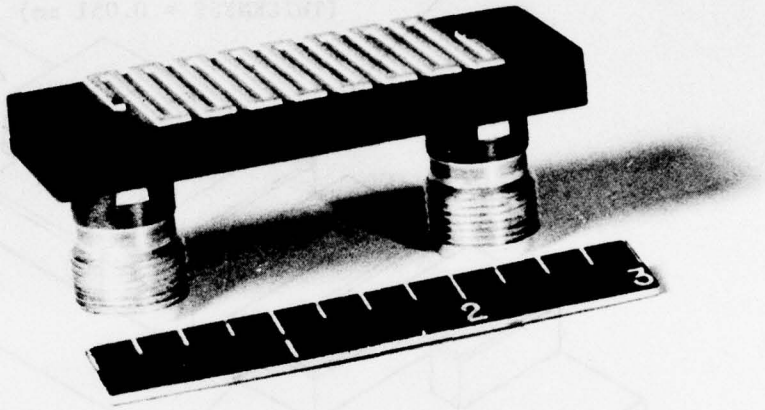

Figure 22. L-Band APS SSML on Spinel

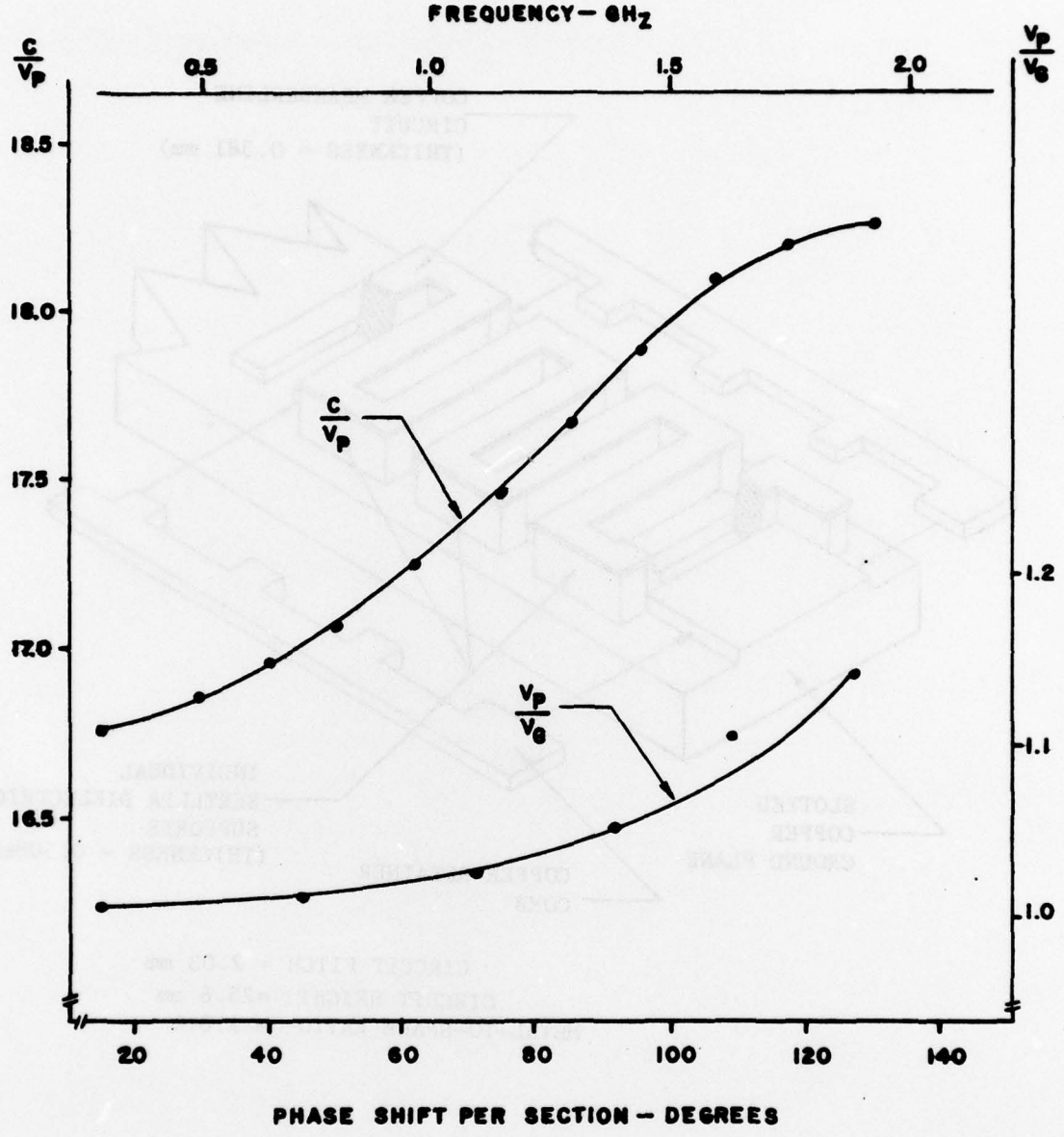

Figure 23. Dispersion Curves for APS-SSM No. 1

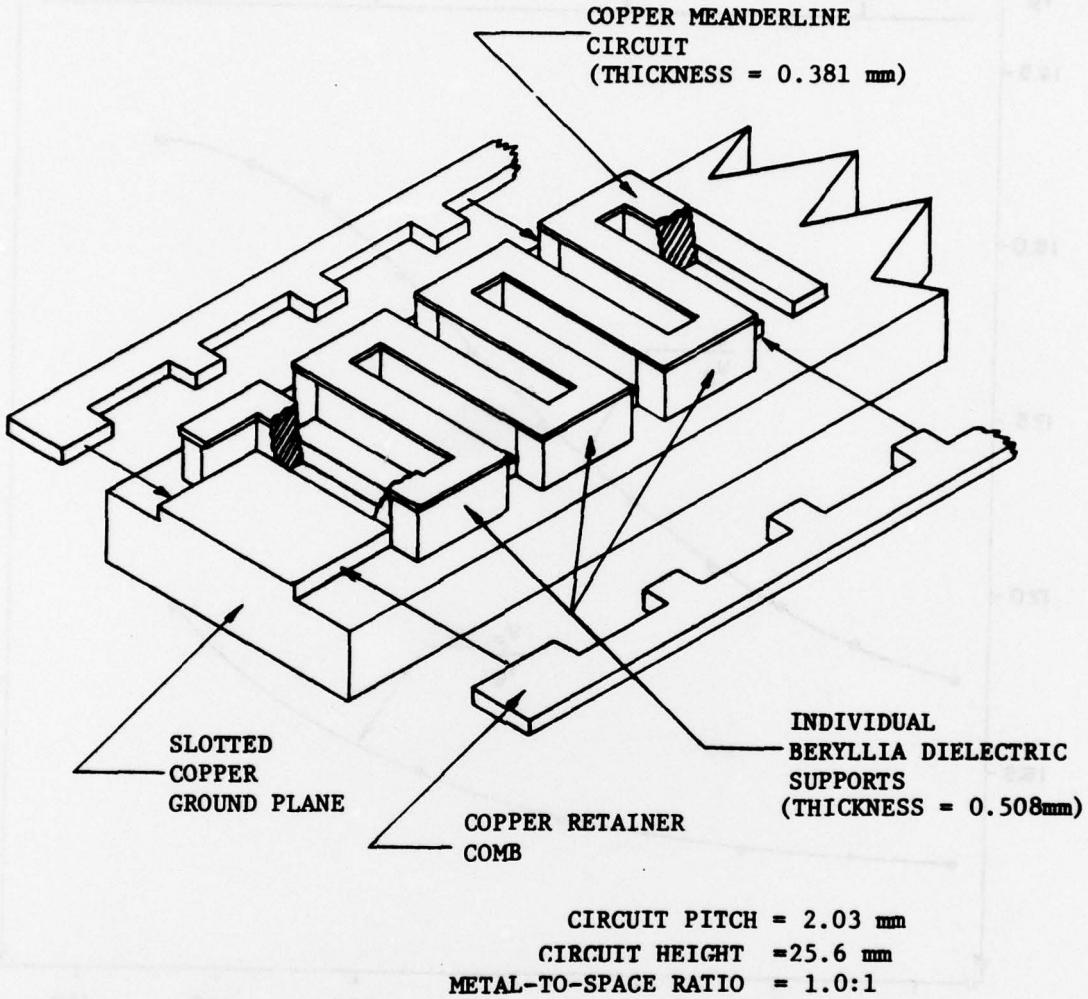

Figure 24. Northrop Simulated L-Band SSML Configuration

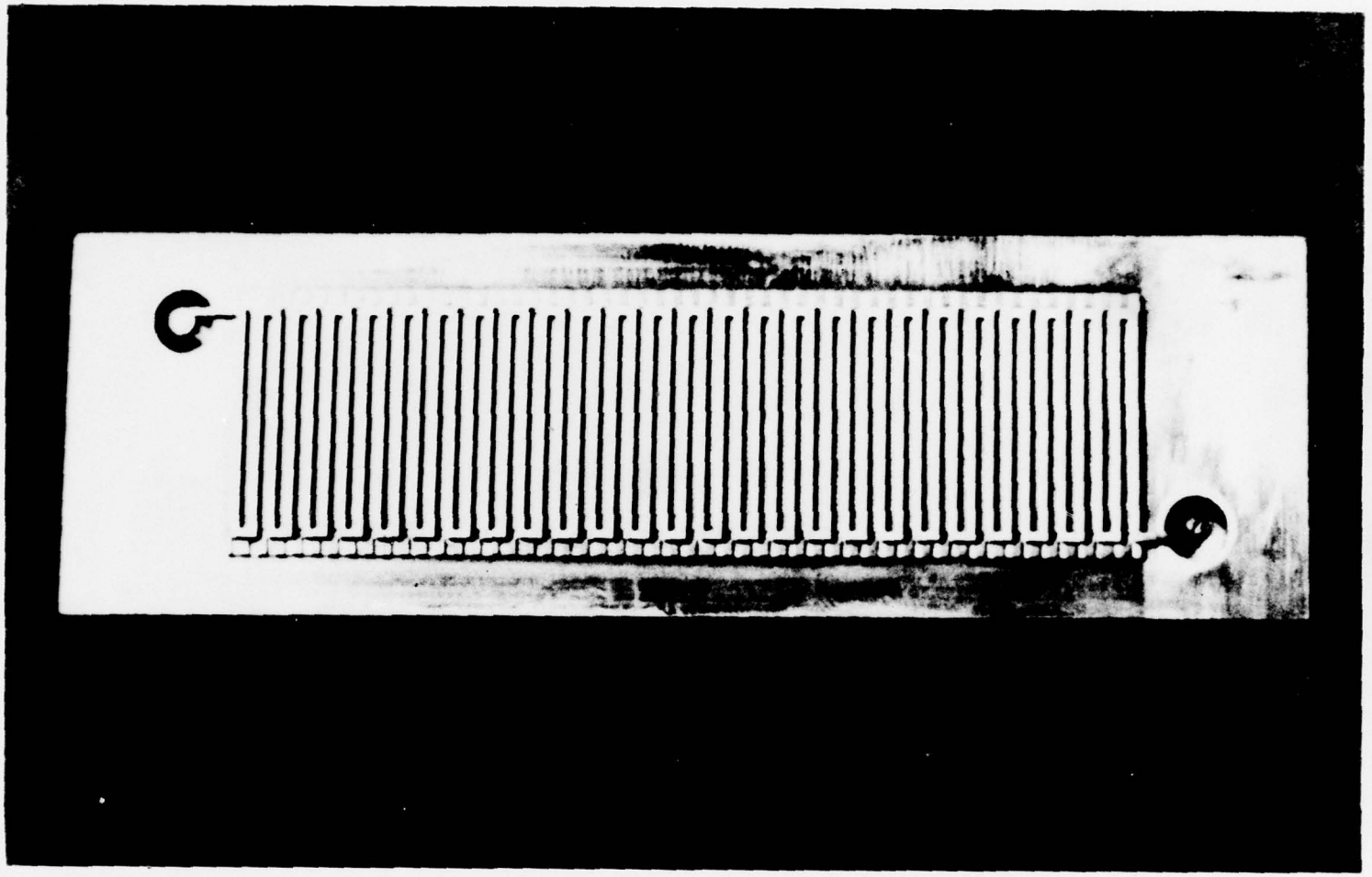

Figure 25. Northrop Simulated L-Band SSML
(Top View)

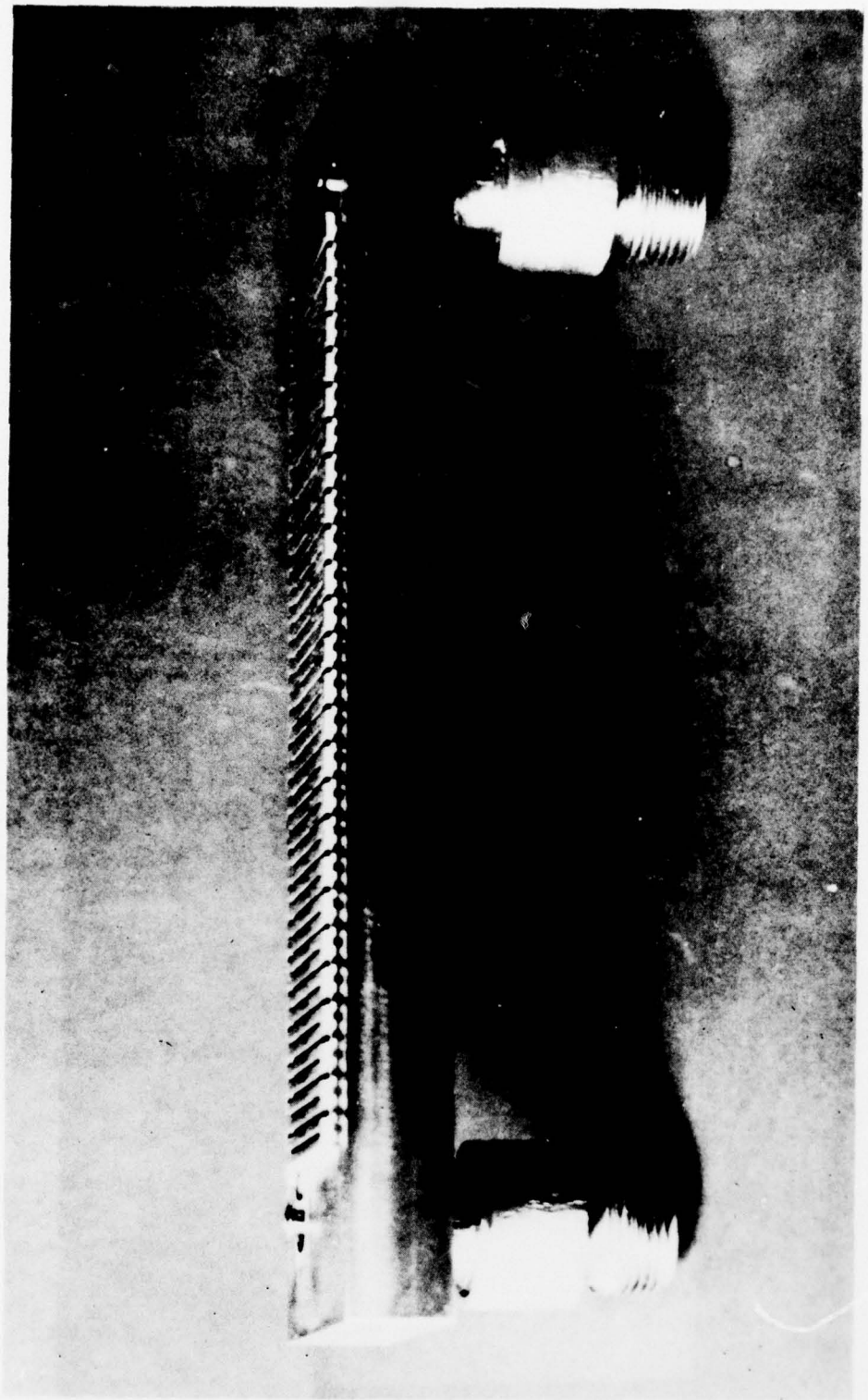

Figure 26. Northrop Simulated L-Band SSML (Side View)

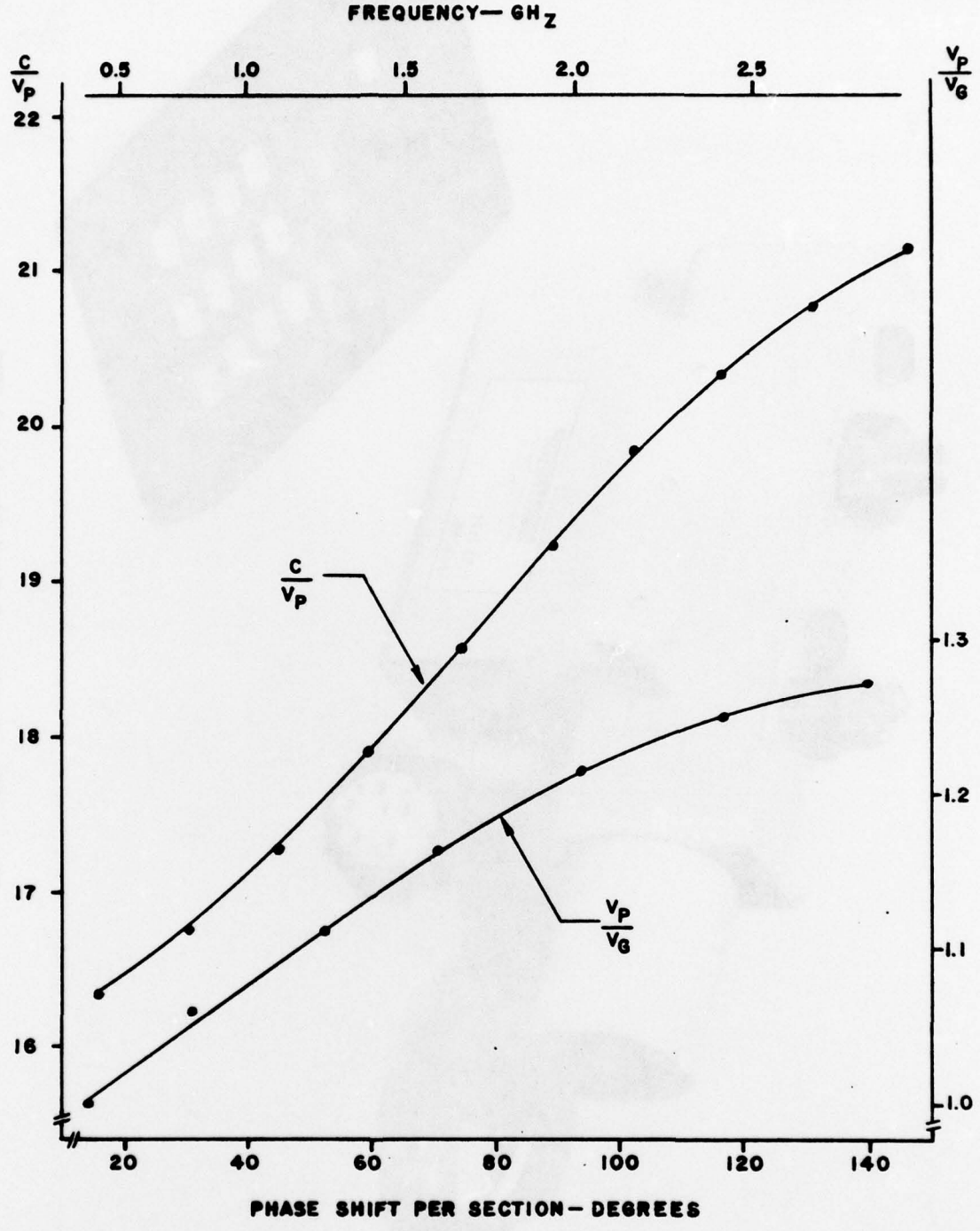

Figure 27. Dispersion Curves for Northrop Simulated SSML

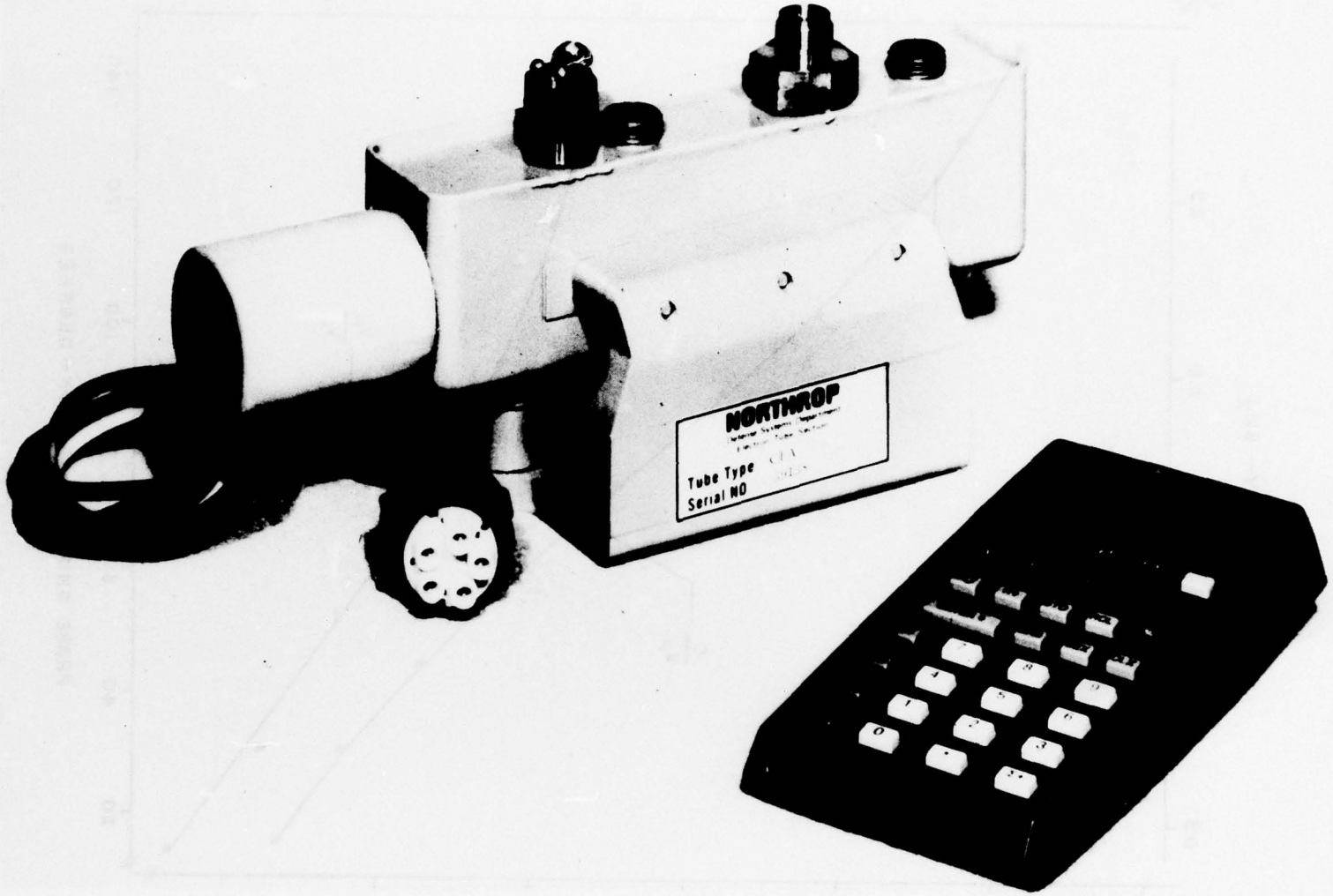

Figure 28. Northrop S-Band Simulated SSML
Hot Test Model

TABLE 1

General Circuit Parameters

Parameter	Symbol	Unit
Frequency	f	sec^{-1}
Phase delay factor	τ or c/v_p	
Phase velocity	v_p	meters/sec
Group velocity	v_g	meters/sec
Interaction impedance	K_i	ohms
Propagation constant	β	radians/meter
Characteristic impedance	Z_o	ohms
Attenuation	α	decibels/meter
Voltage standing wave ratio	VSWR	

TABLE 2

Geometrical Parameters for L-Band CSML

Number of sections	29
Circuit pitch	3.175 mm
Circuit length	92.08 mm
Circuit height	31.75 mm
Slot width	1.420 mm
Vane width	1.755 mm
Metal-to-space ratio	1.24:1
Substrate relative dielectric constant(ε_r)	2.3
Dielectric substrate thickness	0.64 mm
Conductor thickness	0.04 mm

Table 3

Geometrical Parameters for Direct-Bonded-Copper S-Band CSML

Number of sections	30
Circuit pitch	1.27 mm
circuit length	38.1 mm
Circuit height	12.7 mm
Slot width	0.635 mm
Vane width	0.635 mm
Metal-to-space ratio	1:1
Substrate relative dielectric constant(ε_r)	9.6
Dielectric substrate thickness	0.635 mm
Conductor thickness	0.254 mm

Table 4

Geometrical Parameters for SSML #2 & 3 L-Band on Polyguide

	#2	#3
Number of sections	32	30
Circuit pitch	3.175	3.175 mm
Circuit length	101.6	96.83 mm
Circuit height	32.0	33.0 mm
Slot width	1.547	1.547 mm
Vane width	1.628	1.628 mm
Metal-to-space ratio	1.05:1	1.05:1
Substrate relative dielectric constant (ε_r)	2.3	2.3
Dielectric substrate thickness	0.574	0.523 mm
Conductor thickness	0.0355	0.0355 mm

TABLE 5

Dimensional and Electrical Properties of the Experimental Cold Test Circuits

	Pitch (mm)	Height (mm)	Conductor Thickness (mm)	Substrate Material	Substrate Thickness (mm)	BW	α		K_i	Z_o
							Actual	Theor.		
L-Band CSML	3.18	31.8	0.04	Polyguide $\varepsilon_r = 2.3$	0.640	1200	1.03	1.03	71	55
S-Band CSML (DBC)	1.27	12.7	0.254	Alumina $\varepsilon_r = 9.6$	0.635	350	3.75	3.31	22	50
L-Band SSML No. 2	3.18	32.0	0.035	Polyguide $\varepsilon_r = 2.3$	0.574	1150	0.98	0.98	85	55
L-Band SSML No. 3	3.18	33.0	0.035	Polyguide $\varepsilon_r = 2.3$	0.523	1300	1.04	1.08	85	50
S-Band SSML No. 4	2.54	21.34	0.036	Polyguide $\varepsilon_r = 2.3$	0.422	2200	1.52	1.47	72	50
L-Band SSML (APS)	3.18	25.4	0.051	Spinel $\varepsilon_r = 6.46$*	0.762	900	4.16	2.55**	23	40
Northrop L-Band Simulated SSML	2.03	25.6	0.381	Stycast Hi-K6 $\varepsilon_r = 6.0$	0.508	500	NOT MEASURED--	1.73	55	50

*Spinel-Magnesium aluminate $\varepsilon_r = 8.4$. Material used was 80% density with calculated $\varepsilon_r = 6.46$

**The measured high resistivity of the gold spray modified the basic α from 1.52 to 2.55 dB/meter

BW - instantaneous bandwidth in MHz
α - attenuation @ 1.5 GHz in dB/meter
K_i - interaction impedance @ $\Theta = 90°$ in ohms
Z_o - characteristic impedance in ohms

TABLE 6

Geometrical Parameters for S-Band SSML #4 on Polyguide

Number of sections	35
Circuit pitch	2.54 mm
Circuit length	87.7 mm
Circuit height	21.34 mm
Slot width	1.35 mm
Vane width	1.19 mm
Metal-to-space ratio	0.88:1
Substrate relative dielectric constant (ε_r)	2.3
Dielectric substrate thickness	0.422
Conductor thickness	0.036

TABLE 7

Geometrical Parameters for APS L-Band SSML on Spinel

Number of sections	16
Circuit pitch	3.18 mm
Circuit length	50.8 mm
Circuit height	25.4 mm
Slot width	1.59 mm
Vane width	1.59 mm
Metal-to-space ratio	1.0:1
Substrate relative dielectric constant *(ε_r)	6.46
Dielectric substrate thickness	0.762 mm
Conductor thickness	.05 mm

*Spinel - Magnesium Aluminate $\varepsilon_r = 8.4$
Material used was 80% density with
calculated $\varepsilon_r = 6.46$

TABLE 8

Geometrical Parameters for Northrop L-Band Simulated SSML on Stycase 6

Number of sections	51
Circuit pitch	2.032 mm
Circuit length	101.60 mm
Circuit height	25.60 mm
Slot width	1.016 mm
Vane width	1.016 mm
Metal-to-space ratio	1.0:1
Substrate relative dielectric constant (ε_r)	6.00
Dielectric substrate thickness above ground plane*	0.508 mm
Conductor thickness	0.381 mm

* Individual ceramic semgents were located in 0.254 mm deep ground plane grooves

TABLE 9

Geometrical Parameters for Northrop S-Band Simulated SSML on Beryllia Dielectric

Number of sections	62
Circuit pitch	1.22 mm
Circuit length	76.2 mm
Circuit height	14.63 mm
Slot width	0.61 mm
Vane width	0.61 mm
Metal-to-space ratio	1.0:1
Substrate relative dielectric constant (ε_r)	6.6
Dielectric substrate thickness above ground plane*	0.30 mm
Conductor Thickness	0.20 mm

*Individual ceramic segments were located in 0.445 mm ground plane grooves

TABLE 10

Hot Test Results of Northrop S-Band Simulated SSML

Power output (peak)	3.1 kW
Duty	10 %
Power output (average)	300 Watts(W)
Instantaneous bandwidth (one sole voltage)	1000 MHz
Total frequency range with sole tuning	2.0 - 4.0 GHz
Cathode voltage	7 kilovolt (kV)
Beam current (peak)	1.5 ampere (A)
Gain	19 dB
Efficiency (neglecting drive)	30 %
Magnetic field	2700 gauss (G)